UNIVERSITÀ DEGLI STUDI DI MILANO - BICOCCA
Dipartimento di Fisica
Facoltà di Scienze Matematiche, Fisiche e Naturali
Corso di Laurea Specialistica in Fisica

Study of relevant parameters of GEM-based detectors

24/09/2007

Internal Supervisor: Prof. Dt. Stefano Ragazzi

External Supervisor: Prof. Dt. Fabio Sauli

Gabriele Croci
Matricola: 078940

Academic Year 2006-2007

Contents

Acknowledgements

The first person to whom I want to say thank you is Leszek Ropelewski, my CERN supervisor. He followed me in all the lab activities, being very patient with me (mainly at the beginning) and teaching me a lot of things. Thank you very much Leszek and I hope to continue working with you in the future. Then of course I have to say thank you to Fabio Sauli to have given me the possibility to attend the thesis at CERN, to have followed me in the writing-up and correction of this thesis and to have written the first paper including my name. And of course, Fabio thank you for all the clever ideas you always give us. I want to say thank you also to Rob Veenhof for all the hours we spent togheter to solve the simulations problem. I want to thank also to my laboratory collegues David Watts, Serge Duarte Pinto and Elena Rocco for all the discussion we had on different subjects and, I hope, we will continue to have in the future. Thanks also to Miranda Van Stenis, our very precious technician, for all the material you provided me to complete my projects. I want also to say thank you to Jose Mulon (ou probablement c'est mieux dire merci beaucoup Jose) and to Eric David. Thank you very much also to Stefano Ragazzi, my university thesis supervisor.

Ringraziamenti

Voglio cominciare a ringraziare i miei genitori (mamma Mercedes e papá Sergio) per aver reso possibile questa avventura e avermi sostenuto sempre nei momenti di difficoltá e per continuare a farlo sempre. Inoltre devo ringraziare i miei zii (Emilio e Luisa) e mio cugino Maurizio per aver sempre creduto in me. Poi sicuramente devo ringraziare Barbara e Sam per questi mesi passati insieme in quel di Thoiry dove credo ci siamo divertiti (soprattutto nei week-end dove l'attivitá principale era dormire e mangiare studiando di tanto in tanto...). Sono contento di avervi conosciuto meglio. Ora posso ringraziare tutte le altre persone che mi hanno aiutato con la loro presenza e non solo durante il periodo universitario e precedente all'universitá. Comincio a ringraziare Lara per tutto ció che abbiamo passato insieme (soprattutto l'ultima vacanza) e per essere una grandissima persona ed avermi sempre voluto bene. Alessandro grazie anche a te, ormai la nostra amicizia é maggiorenne e credo che basti per dire tutto. Massi come posso esprimere ció che voglio dirti, non ci sono parole tranne una (te vogli beno). Hermann sono contento di averti conosciuto molto bene: sei veramente un grande amico e una persona con cui mi diverto moltissimo. Alex grazie anche a te per essermi stata amica e avermi aiutato ad uscire dal mio primo stato di timidezza. Grazie Ela anche se credo ormai lontana (e lo spero per il tuo futuro) sei una magnifica persona. E infine (di questo gruppo intendo) grazie Fede intendo di tutto, come ti ho giá detto la vacanza dell'anno scorso é stato qualcosa di fondamentale per crescere e per affrontare bene la mia avventura al CERN. Poi devo dire alivraé a Maffe e soprattutto tabbbozzo e bbbabbbuccia ad Alice, subbaqqui/zezzorco a Ste, e ...ti ricordi di me??? a Cami o Camo, grazie anche a voi. Grazie anche a Davide (accelerazioni finali) ed Arianna. Grazie anche a Chiara per tutte le serate passate insieme al libra. Infine devo ringraziare tutti i miei compagni di universitá: Chicco (mitico compagno di tesi al terzo anno), Giacomo, Luca, Alessandra, Dario, Simo, Franco, Davide, Vale, Frate, e spero di non essermi dimenticato nessuno. Grazie ancora a tutti.

Introduction

The main subject of this thesis work is the study of fundamental proprierties of gaseous detectors based on the GEM technology. This is an introduction to the projects I followed during my thesis period at CERN in the GDD group.

The Gas Electron Multiplier consists of a thin Kapton insulating foil copper-clad on both sides and perforated by a high density, regular matrix of holes (50 to 100 per square millimeter). Typically the distance between holes (pitch) is 140 μm and diameters of about 70 μm. The mesh is realised by conventional photolitographic methods as used for the fabrication of multi-layer board. Upon application of a potential difference between the GEM electrodes, a high dipole field develops in the holes focusing the field lines between the drift electrode and the readout element. Electron drift along the channel and the charge is amplified by a factor that depends on the field intensity and the length of the channel. Localization is performed recording the charge reaching a suitably striped or padded electrode. Owing to their excellent position resolution and rate capability GEM-based detector are very suitable to be used in different applications: from the high energy physics to the medical field. In this way I followed two projects: the first one has the goal to better undertand the GEM behaviour (for general GEM applications but in particular for high energy physics application) and the second one was thightly linked to application in medical physics. As fisrt project, the GEM temporal and rate gain stability was studied and it was discovered that the gain variations do not exceed about 20%. Two main phenomena are responsible for the gain variation: the charges movement inside the Kapton after the application of a potential difference and the effect of the external radiation. The charges movement within the Kapton imply a global gain increase in all the GEM area, while the radiation induce a local gain decrease. The first effect is visible measuring the gain immediately after supplying HV to the detector, while the second one is visible only after the GEM has been powered for some hours. Different kinds of GEM geometries (different type of etched GEMs) were tested but the gain variation was

always present. It was found out that triple and single GEM structures behave differently: some physical phenomena present in the triple GEM do not show up in the single GEM. The second project was the development and test of a new kind of GEM-based detector for future On Beam-PET applications. The objective of this new kind of detector is the detection and localization of high energy photons making use of an appropriate mesh converter sheet in front of a GEM device used for charge amplification. To compensate for the low conversion efficiency of a single element, multi-layer structures are needed, with stacks of converter-GEM modules. To ensure that the charge collected does not depend on the position of interaction each cell has to have high local gain but a very low mesh electronic transparency (ϵ) achieving a global cell gain of one. To allow detection of the interaction layer, each cell has to have a large gain and low transfer efficiency, so that their product is unitary (GEM-Gain $= 1/\epsilon$). The depth of interaction is measured knowing which layer is the first to give a signal. The other two coordinates are obtained by conventional methods of charge recording on strips or pads on the last electrode. The test detector used to prove the operating principle was composed by only two cells and it was tested with X-Rays (8.9 keV). The mesh (50 μm hole diameter, 400 μm pitch, 1.2% optical transparent) was not used as converter. A condition of unitary cell gain was determined and the principle was proven measuring separately the GEMs gain and the mesh electronic transparency. The present best unitary cell gain condition achieve a GEM gain of about 350 and a mesh electronic transparency around 0.0033.

Chapter 1

Particle and Matter Interactions

1.1 Interaction of charged particles with matter

A charged particle passing thought a medium (usually gas or solid matter) can interact with it through three different forces: the weak, the strong and the electromagnetic. The electromagnetic one is by far the most likely to occur because it is several order of magnitude more probable. The weak interaction usually play a fundamental role in detection of extremely elusive particle such as the neutrinos; the strong one usually concerns only the detection of neutron (particularly nuclear reaction producing charged particle from an incoming neutron) The Coulomb interactions between incoming particle and matter lead to two important phenomena: the excitation and the ionization of the atoms of the medium. Ionization means the creation of an electron-positive ion pair while excitation means the change of an atom to an higher energy status. Excitation can also produce electron from the de-exciting processes. All these produced electrons are called primary ionization electrons. In addition, if these electrons can acquire additional energy (in presence of an external electric field) they can further ionize creating the so called secondary delta electrons. Usually a charged particles leaves a track in a medium and creates cluster of ions/electrons. Other electromagnetic process, such as Bremsstrahlung, Čerenkov and transition radiation may occur; but in a case of a gaseous detector (the main framework treated in this report) they are negligible and can be ignored.

1.1.1 The Bethe-Bloch Formula

The electromagnetic energy loss of heavy ($m >> m_e$) charged particles in matter is a statistical process involving many successive discrete interactions.The *linear stopping power S*

in a given absorber is defined as the differential loss for that particle within the material divided by the corresponding differential path length: $S = -\frac{dE}{dx}$. The classical expression that describes the specific energy loss (that is the value of -dE/dx along a particle track) is known as the Bethe-Bloch formula and is written

$$-\frac{dE}{dx} = \frac{4\pi e^4 z^2}{m_0 v^2} NZ \left[\ln \frac{2m_0 v^2}{I} - \ln\left(1-\beta^2\right) - \beta^2 \right] \tag{1.1}$$

where v and ze are the velocity and the charge of the incoming particle, N and Z are the number density and atomic number of the absorber atoms, m_0 is the electron rest mass and e is the unit electronic charge. The parameter I stands for the average excitation and ionization potential of the absorber and is normally treated as an experimentally determined parameter for each element. This average value can be parameterized as $I \approx I_0 Z^{0.9}$ with $I_0 \approx 12$ eV. Equation 1.1 is generally valid for different types of charged particle provided that their velocity is large compared with the velocity of the orbital electrons of the absorbing atom.

The Bethe Bloch Formula has a very important feature: its minimum (≈ 2 MeV $g^{-1}cm^2$ at a value of $\beta \approx 0.95$) is almost independent from the target medium. Always relativistic particles have energy-losses near to this minimum. This particles are called Minimum Ionizing Particle (MIPs). Particles with energy lower than these MIPs loses a large amount of their energy ($\frac{1}{v^2}$ dependence in the Bethe-Bloch Formula). For higher energy than MIPs the energy-loss rises only slightly due to the large energy transfer to few electrons.

If the absorber medium is composed by a mixture of elements (this is the case of gas mixtures) the Bethe-Bloch Formula is still valid if the respective losses are added taking into account the appropriate weighting factors of the components.

1.1.2 Energy Loss Distribution

The electromagnetic loss is a result of a number of discrete interactions and, therefore, is a statistical process and is usually described with a mean value. The distribution is not Gaussian for all the cases where the energy loss ΔE is small compared to the total energy. For thin material (this can be the case of a small gas gap) the energy loss distribution is well described by the Landau expression

$$f(\lambda) = \frac{1}{\sqrt{2\pi}} \cdot e^{-\frac{1}{2}\left(\lambda + e^{-\lambda}\right)} \tag{1.2}$$

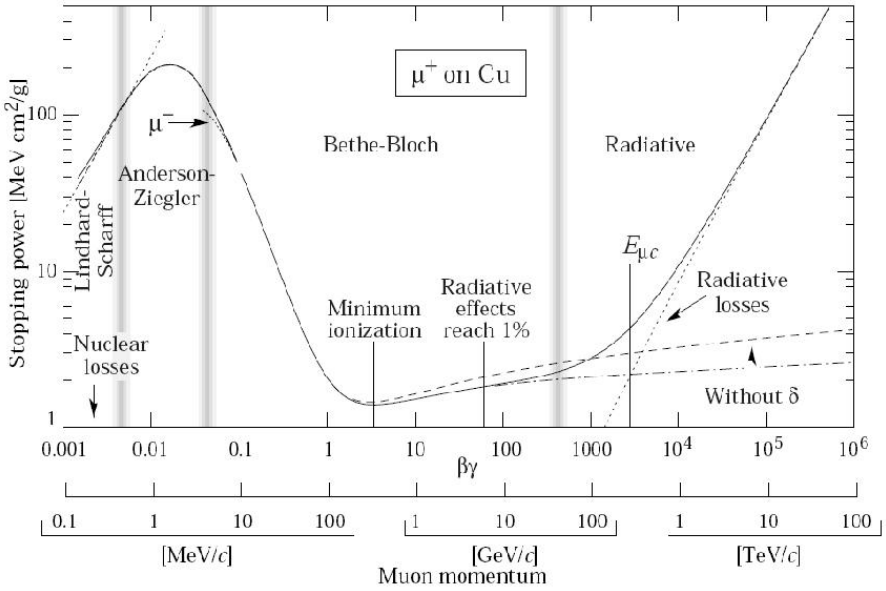

Figure 1.1: The Plot of the Bethe-Bloch Formula, [Kno99]

where the reduced energy variable λ represents the normalized deviation from the most probable energy loss (ΔE_{mp}):

$$\lambda = \frac{\Delta E - \Delta E_{mp}}{\xi}$$

where ΔE is the real loss and ξ is the average energy loss given by the first term in the Bethe-Bloch Formula.

The Figure 1.2 shows the characteristic shape of the Landau distribution and indicates the meaning of the average and of the most probable energy losses. A long tail is very visible at very large energy losses corresponding to events where one or more energetic δ electrons have been produced: these particular electrons are electrons with very high energy that can even escape from the detection region.

The large fluctuation in the energy loss for individual events has important critical consequences mainly in designing the detector amplification electronics which has to be able to take into account the large dynamic range of the signal.

1.1.3 Primary and total ionization

A close look to the interaction phenomena shows that close collision, with large energy transfer results in primary ionization (liberation of electronic charges, in particular pairs of electron/positive ion) while distant collision involve smaller energy transfer and can mainly result

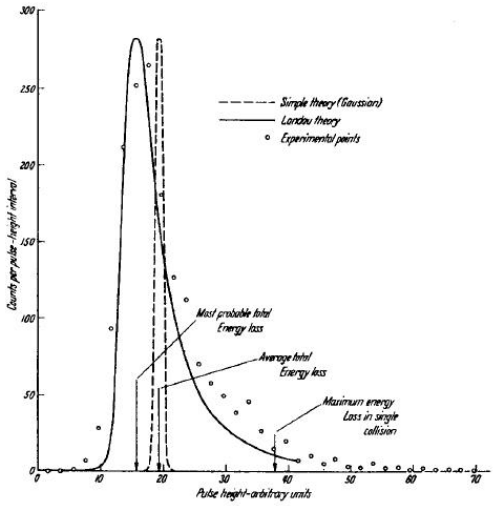

Figure 1.2: Landau Distribution, [Sau77]

in excitation. The electron emitted after a ionization process can have enough energy to further ionize, producing secondary pairs of electrons-ions; the sum of the primary and secondary ionization is called Total Ionization. The total number of charged pairs can be expressed as

$$n_T = \frac{\Delta E}{W_i} \tag{1.3}$$

where ΔE is the total energy loss in the volume considered and W_i is the average energy to produce one pair. For our experimental purposes we are interested in knowing the total ionization produced by photoelectron created by X-Rays from Cu (8.9 KeV) and Fe (5.9 KeV) (copper and iron cathode tubes) that will be the two main sources thought all the measurements performed. Further we will calculate this for the mainly used gas mixture: Ar 70% CO_2 30%. Using the values reported in table 1.1.3 ([Sau77]) and weighting the two values respect to the percentage contain we obtain for Cu X-Rays

$$n_{tot} = \frac{5900}{26} \cdot 0.70 + \frac{8900}{33} \cdot 0.30 \approx 320 \text{ pairs} \tag{1.4}$$

and for Fe X-Rays

$$n_{tot} = \frac{5900}{26} \cdot 0.70 + \frac{5900}{33} \cdot 0.30 \approx 213 \text{ pairs} \tag{1.5}$$

where we used $W_i(Ar) = 26$ eV and $W_i(CO_2) = 33$ eV.

Gas	Z	A	δ (g/cm³)	E_{cx}	E_i (eV)	I_0 (eV)	W_i	dE/dx (MeV/g cm⁻²)	dE/dx (keV/cm)	n_p (i.p./cm) a)	n_T (i.p./cm) a)
H_2	2	2	8.38×10^{-5}	10.8	15.9	15.4	37	4.03	0.34	5.2	9.2
He	2	4	1.66×10^{-4}	19.8	24.5	24.6	41	1.94	0.32	5.9	7.8
N_2	14	28	1.17×10^{-3}	8.1	16.7	15.5	35	1.68	1.96	(10)	56
O_2	16	32	1.33×10^{-3}	7.9	12.8	12.2	31	1.69	2.26	22	73
Ne	10	20.2	8.39×10^{-4}	16.6	21.5	21.6	36	1.68	1.41	12	39
Ar	18	39.9	1.66×10^{-3}	11.6	15.7	15.8	26	1.47	2.44	29.4	94
Kr	36	83.8	3.49×10^{-3}	10.0	13.9	14.0	24	1.32	4.60	(22)	192
Xe	54	131.3	5.49×10^{-3}	8.4	12.1	12.1	22	1.23	6.76	44	307
CO_2	22	44	1.86×10^{-3}	5.2	13.7	13.7	33	1.62	3.01	(34)	91
CH_4	10	16	6.70×10^{-4}		15.2	13.1	28	2.21	1.48	16	53
C_4H_{10}	34	58	2.42×10^{-3}		10.6	10.8	23	1.86	4.50	(46)	195

a) i.p. = ion pairs

1.2 Interaction of photons with matter

The photon, being a neutral particle, interacts differently from the charged particle. In fact, on the contrary of a continuous energy loss for the charged particle, the neutral ones lose the totality or a part of their energy in a single process. For photons it is important to consider the probability of interaction: a photon beam passing through a medium of thickness X and with N molecules per unit volume, has an attenuation described by

$$n = n_0 e^{-\sigma N X} = n_0 e^{-\mu \rho X} \tag{1.6}$$

where μ is the mass attenuation coefficient thickness and ρ is the density of the absorber. σ is the total cross section of photon-matter interaction and determines the probability of absorption. The total cross section is the sum of three different cross section that describe the three ways of interaction between photons and matter: the photoelectric process, the Compton Scattering and the electron-positron pair production. The three different process dominates at different energy level (see Fig 1.3). Since we worked mainly with photons it is worth to give a more extended explanation of every single process. For the energy region in which we worked (few KeV) the only important one is the Photoelectric Absorption.

1.2.1 Photoelectric effect

This is the dominant process for energy under 500 KeV. In the photoelectric effect, a photon undergoes an interaction with an absorber atom in which the photon completely disappears. In its place. an energetic photoelectron is ejected by the atom from one of its bound shells. This process has a threshold: if E_γ the energy of the incoming photon and E_b the boundary

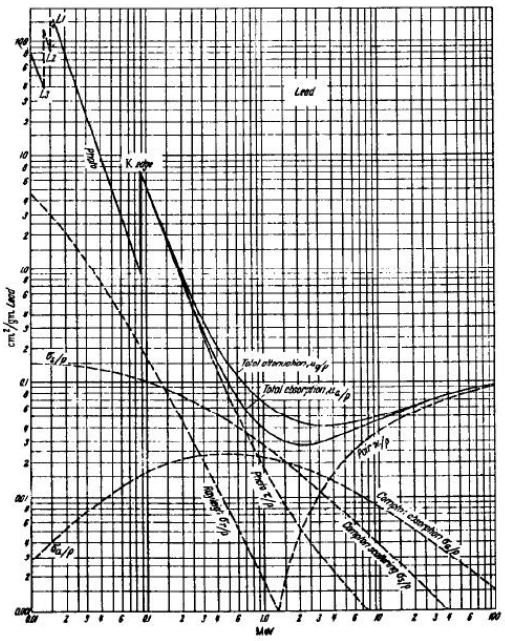

Figure 1.3: General Plot of the total photon cross section, [Sau77]

energy of the electron, only if $E_\gamma > E_b$ the photoelectron is emitted with an energy E_e

$$E_e = E_\gamma - E_b \tag{1.7}$$

For photon energies up to about 20KeV the direction of the photoelectron is nearly orthogonal to the direction of incident photon. Together with the photoelectron, the process also creates an ionized absorber atom with a vacancy in one of its bound shells. This vacancy is quickly filled through capture of a free electron from the medium and/or rearrangement of electrons from other shells of the atom. Therefore one or more characteristic X-ray photons may also be generated. Although in most cases these X-Ray are reabsorbed close to the original site through photoelectric absorption involving less tightly bound shells, their possible escape from the sensitive volume of radiation detectors can influence their response, giving sight into the so called *Escape Peak*.The fraction of de-excitation producing a photon is called fluorescence yield. In some fraction of the cases it is possible to have de-excitation with the emission of an Auger electron that carries away the excitation energy. In Argon, for example, about 15% of the photoelectric absorptions are followed by the emission of a photon while in the 85% of the events two electron are produced.

1.2.2 Compton Scattering

Compton scattering takes place between an incident photon (of at least 1 MeV energy, more than the highest atomic energy level) and an electron, the latter assumed to be initially at rest. In the Compton effect the incoming photon is deflected through an angle θ respect to its original direction; the photon transfers a portion of its energy ($h\nu$) to the electron which recoils. The energy of the scattered photon is given by:

$$h\nu^{'} = \frac{h\nu}{1 + \frac{h\nu}{m_o c^2}(1 - cos\theta)} \tag{1.8}$$

where m_0 is the electron mass. The angular distribution of the scattered photon is predicted by the Klein-Nishina formula for the differential cross section:

$$\frac{d\sigma}{d\Omega} = Z r_o^2 \left(\frac{1}{1 + \alpha\,(1 - cos\theta)}\right)^2 \left(\frac{1 + cos^2\theta}{2}\right) \cdot \left(1 + \frac{\alpha^2\left(1 - cos^2\theta)^2\right)}{((1 + cos^2\theta)\,(1 + \alpha\,(1 - cos\theta))}\right) \tag{1.9}$$

Where $\alpha = h\nu/m_o c^2$ and r_o is the electron classical radius.

1.2.3 Electron-Positron Pair Production

If the photon energy exceeds twice the rest-mass energy of an electron (1.022 MeV) the process of electron-positron pair production is energetically possible. As practical it increases very fast above threshold. It becomes the dominant effect for energy over 10 MeV.

Chapter 2

Drift and diffusion of particles in gas

This chapter deals with the creation of a toy model that describes drift and diffusion of particles in non-homogeneous fields (with convergent or divergent flow). This toy model describes non-physical situations but it will be the base for the introduction of these processes in the real case inside the Gaseous Detector Simulation Program **Garfield**.

2.1 Classical Theory

Electrons and ions in a gas are subject only to a move on average along the electric field ($\overrightarrow{v}_{Drift} = \mu\overrightarrow{E}$, where μ is the particle mobility), but individual electrons deviate from the average due to scattering on the atoms of the gas. Scattering leads to variations in velocity, called longitudinal diffusion, and to lateral displacements, called transverse diffusion. The scattering process in each direction can to a good approximation be considered Gaussian on a microscopic scale. In the presence of both an electric and a magnetic field, the average motion has in general components parallel to E, B_{T}, the component of B which is transverse to E, and to $E \times B$.

In the presence only of an homogeneous electric field in one dimension the law for diffusion of localized charge distribution is:

$$\mathrm{f}(x)\mathrm{d}x = \frac{1}{\sqrt{4\pi Dt}} e^{\frac{(x-x_0)^2}{4Dt}} \mathrm{d}x \tag{2.1}$$

where $\mathrm{f}(x)$ is the fraction of charge found in an element $\mathrm{d}x$ centered in x_0 after a time t,

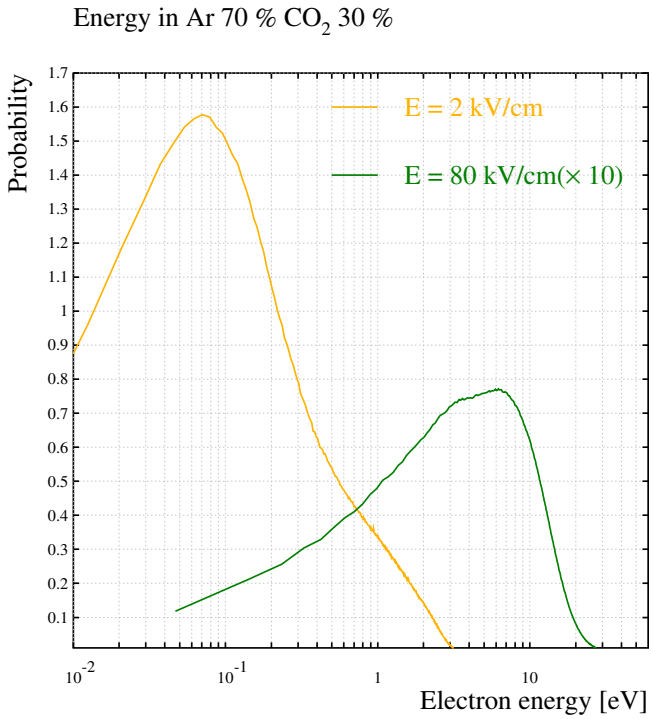

Figure 2.1: Electrons energy distributions in two electric fields: a drift field (2 kV/cm, orange) and a GEM hole field (80 kV/cm, green)

and D is the diffusion coefficient. The diffusion is defined as the RMS [1] of the distribution. The diffusion depends on the gas mixture, on the temperature and on the pressure.

2.2 Electrons energy distribution

The drift electrons, created in an ionisation process, have an energy distribution which depends from the electric field. Fig. 2.1 illustrates the energy distributions of electrons created in the gas mixture $Ar/C0_2$ 70%/30% for two different electric fields. The orange line represents the energy distribution in a usual drift field (2 kV/cm) and the green line in a GEM hole field (80 kV/cm)

Fig 2.2 shows the cross section for different phenomena in the same gas mixture as before.

[1] In a time dependent description:

$$\sigma_x = \sqrt{2Dt} \tag{2.2}$$

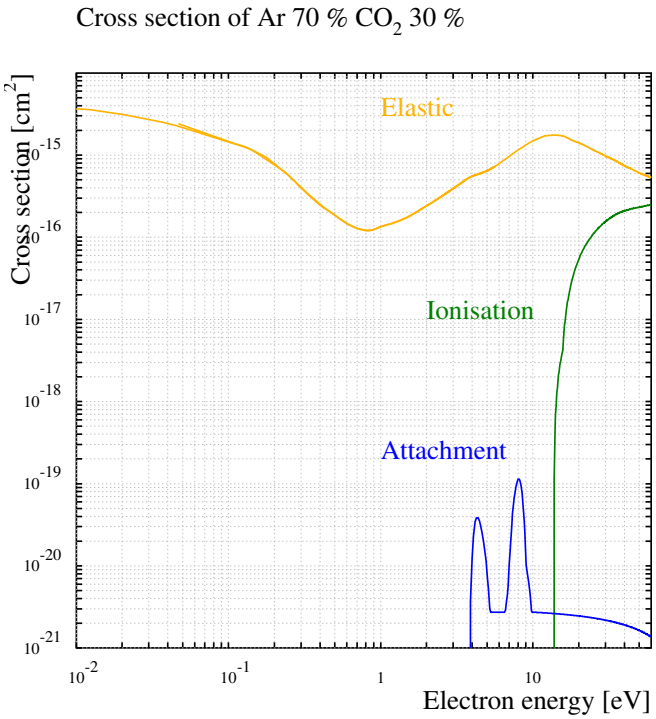

Figure 2.2: Cross sections for different processes in Ar/CO_2 70%/30% from Magboltz [Bia99]

2.3 Present Garfield Implementation Status

In view of the Gaussian nature of the diffusion process, it is natural to describe it in terms of a three-dimensional normal distribution . In the absence of correlations between the diffusion coefficients, the covariance matrix is diagonal in a frame in which the average direction of motion is one of the axes and in which the other two axes are suitably chosen. In an arbitrary frame of reference, or in the presence of physical correlations, however, the covariance matrix will not be diagonal but it will still be symmetric. We therefore add a further 3 coefficients to build a (symmetric) covariance matrix which enables us to formulate the diffusion process independent of a coordinate system. The independence of a coordinate system authorises us to call this matrix the diffusion tensor.

2.3.1 Diffusion Coefficient

Longitudinal and transverse diffusion coefficients have been measured for a variety of pure gases and gas mixtures over a broad range of E fields. Measurements with a B field are scarce however and rarely will one find data for the exact configuration of E and B fields one

needs. It has therefore become usual to rely for these coefficients on calculations, often with Magboltz [Bia99] , a program that simulates all the gas/particle interaction proprierties.

2.3.2 Homogeneous Constant Field

Denoting the diffusion tensor by Σ^{-1}, and assuming homogeneous E and B fields, the probability that a particle is scattered by a vector x with respect to the average direction of motion is given by:

$$P = \frac{1}{2\pi\sqrt{|\Sigma|}} e^{\frac{1}{2}x^T\Sigma^{-1}x} \tag{2.3}$$

Σ fully describes the diffusion process. This tensor depends on E and on B, but also on the mean distance travelled by the particle during the diffusion process. Writing the mean distance over which the particle drifts as d, the diffusion coefficients in each of the directions as σ_x, σ_y, and σ_z and the correlation coefficients as σ_{xy}, σ_{xz} and σ_{yz}, the expression for Σ is:

$$\Sigma = d \begin{pmatrix} {\sigma_x}^2 & \sigma_{xy} & \sigma_{xz} \\ \sigma_{yx} & {\sigma_y}^2 & \sigma_{yz} \\ \sigma_{zx} & \sigma_{zy} & {\sigma_z}^2 \end{pmatrix}$$

This is the natural extension of a 1-dimensional diffusion process, where $\Sigma = \mathrm{d}\sigma^2$

2.4 A Toy Model of transport in inhomogeneous fields

The fields treated in this paragraph are only locally physical: in real detectors diffusion is not constant and divergent fields do not have an increasing velocity going away from the centre of the field. But solving examples like these is very precious to verify the calculations for the general case, which are done numerically. The general calculations will take into account all the full diffusion tensor and transport matrix.

2.4.1 Drift

If the E and B fields are not homogeneous, the mean drift paths from neighbouring points will diverge or converge, while particles may accelerate or decelerate along the mean drift path. A two dimensional simulation program that computes the drift velocity and drift path of an initial Gaussian distribution of electrons was created to understand how to implement the drift and diffusion of particles. A Gaussian distribution in two dimension can be expressed in

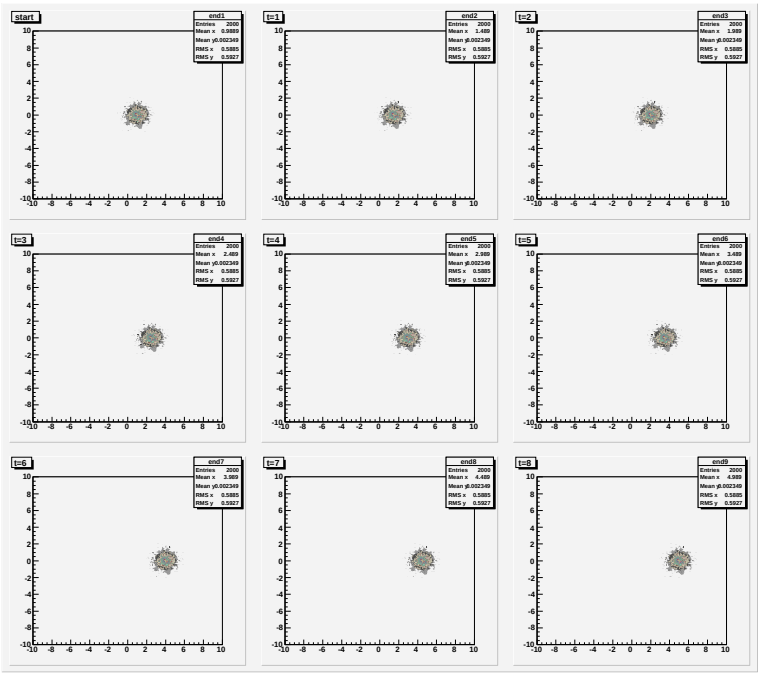

Figure 2.3: Drift in constant Field, E_x=const, E_y=0

term of an ellipse (this is the method that will be used in this report) and in three dimensions in term of an ellipsoid. This simulation program does not take into account the diffusion but only the deformation of the initial Gaussian distribution.

The following fields leave a starting Gaussian cloud unchanged, it means that an ellipse will remain an ellipse maybe with different values of the parameters

1. Constant field; Fig. 2.3 shows that a particle cloud in a constant field (in this case the field is parallel to the x axis) simply moves without changing its distribution shape. The ellipse parameter will remain the same.

2. Radial field in which the particle velocity increases linearly from smaller to larger radius (Fig 2.4). The Gaussian cloud will grow and remain Gaussian.

The following fields are examples of fields that completely transform the initial elliptic shape.

1. Radial field in which the particle cloud has a constant mobility. An originally elliptic cloud becomes a banana shape. The transformation results in a more broadened distribution if the cloud centre is near to the field centre, where the field lines are very dense. Figure 2.6 shows the results.

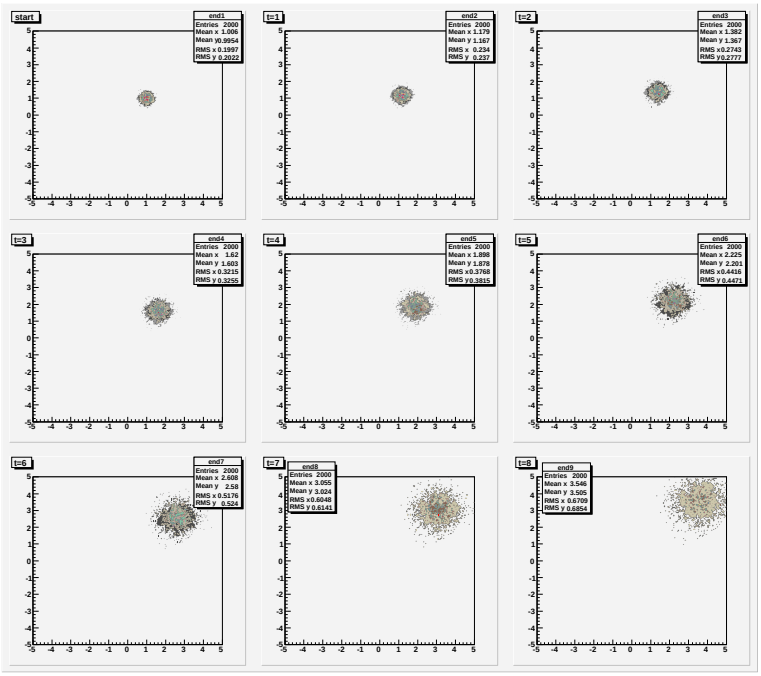

Figure 2.4: A radial field linearly increasing with the distance from the centre

2. Toy model of a GEM-like field. (see Fig 2.5). The field used is not a very high field and thus the avalanche processes are not computed. Only the approximated shape of the GEM field is taken into account. Figure 2.7 shows the shape transformation of an initial Gaussian cloud passing through one GEM-like hole.

.

2.5 Problems and their solution in the toy model

The final distribution obtained in a radial field with constant mobility and in a GEM-like field are not easy to parametrise. Since the only distribution that can be implemented in a simulation program like Garfield is the Gaussian one (or the elliptic one) it is hard to treat the drift processes in non constant field. What we decided to do is to find a way to render the non-Gaussian distribution a Gaussian distribution. We want to search what is the maximum time interval dt in which the cloud can still be considered Gaussian. Once discovered this time interval and consequently the new localisation of the cloud, the parameters for the ellipse are computed in this point. After this the calculation restarts taking the previously calculated parameters as the initial ones. The crucial point becomes now the capability of recognise an

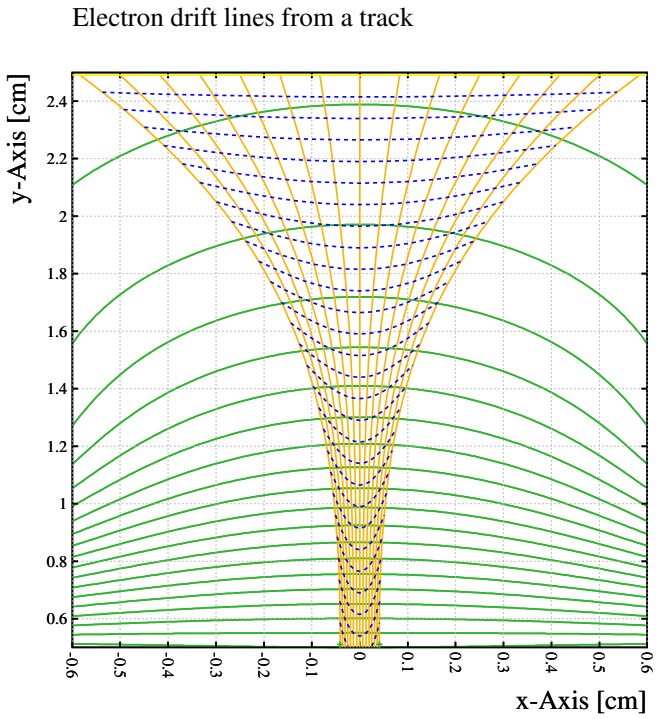

Figure 2.5: TOY MODEL GEM-like field

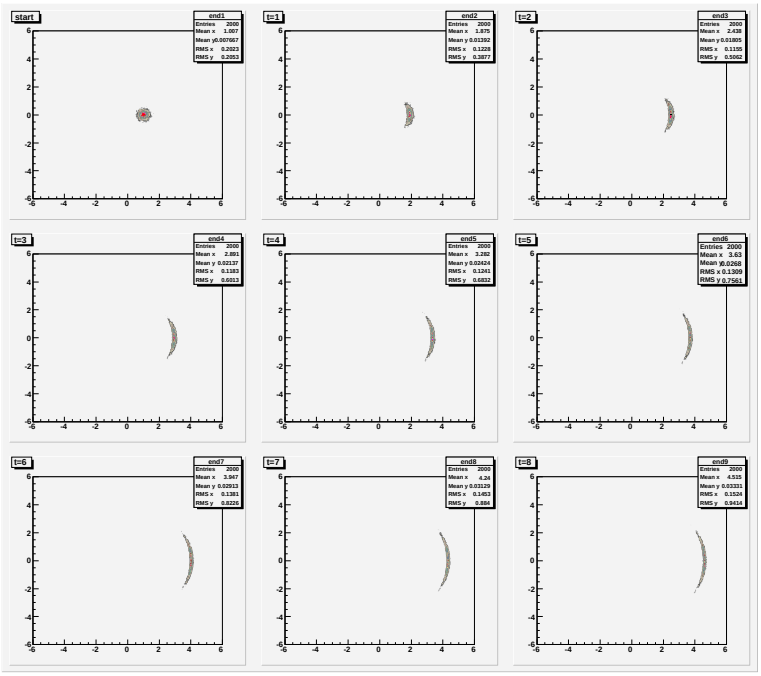

Figure 2.6: Drift in radial field with constant mobility, The field centre is in (0,0)

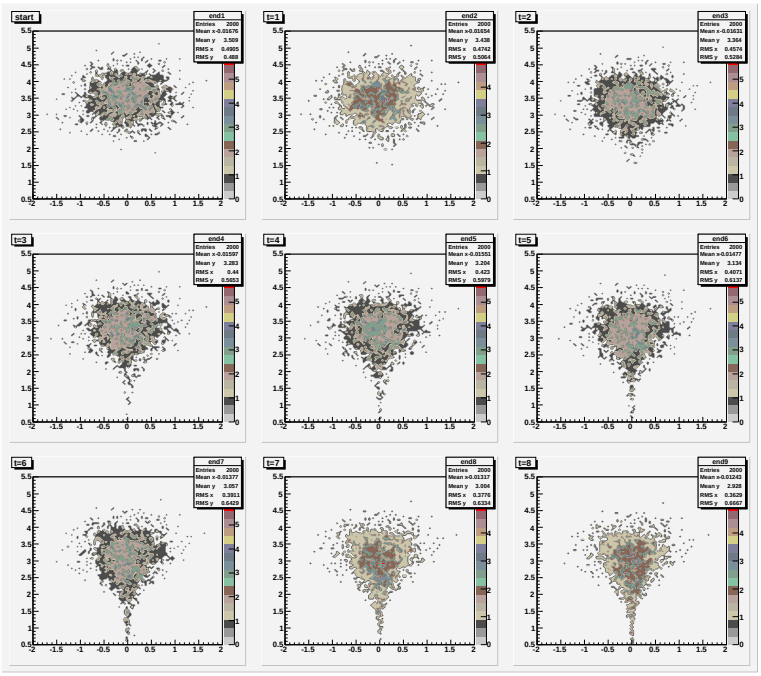

Figure 2.7: TOY MODEL of a gaussian cloud moving in GEM-like Field, the GEM-like hole centre is in (0,0)

ellipse (in two dimension) or the ellipsoid (in three dimensions) given the minimum number of points representing the cloud shape (5 for two dimensions, the centre plus 4 points and 7 for three dimensions). This pattern recognition will give in the end the parameters of the ellipse, that is the parameters of Σ and the degree of *ellipticity* of the cloud.

In particular there are three requirements that must be satisfied:

1. the centre must be inside the area described by the other points;
2. once an order for the points has been decided, they must maintain it;
3. a function describing the distance between the points and a fitted ellipse must be minimised: the value of the minimum will be the ellipticy degree.

The threshold of ellipticity will be user-defined.

2.6 How to include the diffusion in the toy model

So far it has been determined how to explain the spread, given by the drift, of an electric cloud in non-homogeneous fields. The next step is to include the diffusion processes. In the presence of both an electric and a magnetic field these processes are described in a 3-D model by the diffusion tensor S:

$$S = \begin{pmatrix} \sigma_E^2 & \sigma_{E,BT} & \sigma_{E,ExB} \\ \sigma_{E,ET} & \sigma_{BT}^2 & \sigma_{B_T,ExB} \\ \sigma_{E,ExB} & \sigma_{BT,ExB} & \sigma_{ExB}^2 \end{pmatrix}$$

The parameters describe the diffusion terms induced by E and B field. In the absence of a magnetic field or when the electric and magnetic field are parallel, only the transverse diffusion σ_T (two times) is considered instead of σ_{BT} and σ_{ExB}. The diffusion term parallel with the electric field is called longitudinal diffusion σ_L. To determine the total diffusion over a finite length we sub-divide it in steps and calculate the diffusion as the sum sub-steps. If the total distance is $d = d_1 + d_2$, the total diffusion will be $S_d = S_{d1} + S_{d2}$. Now we combine the diffusion with the spread knowing that they happen at the same time.

The following paragraph deals with a diverging radial field in which the velocity of the particles increases linearly going away from the centre and in which it is considered a constant value for the diffusion coefficient: of course this is not a real case but it is important to solve

cases like this to be able to solve more difficult ones. Converging or diverging field are common: a GEM field, in the region below the centre of the hole, has a divergent flow and a single wire counter has a convergent flow.

For real applications, one will of course use the full diffusion tensor and transport matrix.

2.6.1 Two Dimensional Diverging Radial Flow

The toy field we consider in this case is radial flow with velocity increasing linearly from the centre. The effect of the spread in such a field is simply a uniform stretch: it means that an initial elliptic distribution will remain elliptic but its parameters will be changed (see Fig 2.4). Also the diffusion will change the parameters but keeping the elliptic shape. Starting from a point-like distribution the diffusion will turn it in an elliptic (Gaussian) distribution after a while. For simplicity we will treat a circular and not an elliptic distribution. The aim of this exercise is to understand how the radius of a circular distribution will change. Assume that x_0 is the distance between the centre of the field and the centre of the cloud (see 2.8) and that the cloud drifts over a distance d: what will be the radius of the cloud in the end ?

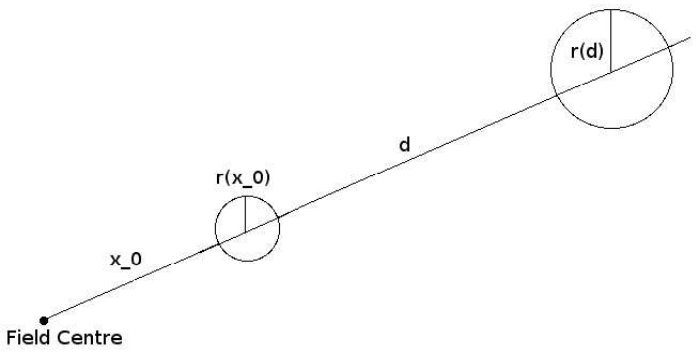

Figure 2.8: Schematic view of the changing of the distribution radius

Now we sub-divide the step of length d into n steps of length $\frac{d}{n} = \delta$ and we let $n \to \infty$ We assume for simplicity $\sigma_T = \sigma_L = \sigma$ and so that the diffusion tensor can be written as:

$$\mathrm{S}_\delta = \delta \begin{pmatrix} \sigma^2 & 0 \\ 0 & \sigma^2 \end{pmatrix} = \delta S$$

.

The radius enlargement factor given by the spread over a distance δ can be expressed as

the ratio between the new distance from the centre of the field and the old one. For the first step it is:

$$\frac{x_0+\delta}{x_0} \tag{2.4}$$

In each step δ the spread will act on the diffusion induced in the previous steps and the same diffusion will be added. The action of the spread on the diffusion is simply represented by the multiplication of the matrix by the radius enlargement factor. The mathematical expression of the sum of the effect in the first step is given by:

$$\frac{x_0+\delta}{x_0}S_\delta + S_\delta = \left(1+\frac{x_0+\delta}{x_0}\right)S_\delta \tag{2.5}$$

The second step will become

$$\left[\left(1+\frac{x_0+\delta}{x_0}\right)S_\delta\right]\frac{x+2\delta}{x+\delta} + S_\delta = \left(1+\frac{x_0+2\delta}{x_0+\delta}+\frac{x_0+2\delta}{x_0}\right)S_\delta \tag{2.6}$$

And for n steps, the following series is obtained

$$\left[1+\sum_{i=0}^{n}\frac{x_0+n\delta}{x_0+i\delta}\right]\delta S \tag{2.7}$$

Now putting $a=\frac{x_0}{\delta}$ the series can be rewritten as

$$\delta\left(1+\sum_{i=0}^{n}\frac{a+n}{a+i}\right)=\delta\left(1+\sum_{i=0}^{n}\frac{(a+i)+(n-i)}{a+i}\right)=\delta\left(1+\sum_{i=0}^{n}1+\frac{n-i}{a+i}\right)=\delta\left(1+n+\sum_{i=0}^{n}\frac{n-i}{a+i}\right) \tag{2.8}$$

And taking the limit

$$\lim_{n\to+\infty}\sum_{i=0}^{n}\frac{n-i}{a+i}=\frac{n^2}{a} \tag{2.9}$$

Now taking expression 2.7 it becomes

$$(1+n+\frac{n^2}{a})\delta\begin{pmatrix}\sigma^2 & 0\\ 0 & \sigma^2\end{pmatrix} \tag{2.10}$$

and considering only the part without matrix and expressing $a=\frac{x_0}{\delta}$ this expression becomes

$$\delta+\delta n+\frac{n^2\delta^2}{x_0} \tag{2.11}$$

.

Taking $n \to \infty$, $\delta \to 0$ and $n\delta = d$

The final expression for the square of the radius change will be

$$\left(d + \frac{d^2}{x_0}\right) I\sigma^2 \tag{2.12}$$

and thus the radius change as a function of drifting distance will be the square root of the previous expression

$$r(d) = \sqrt{d + \frac{\mathrm{d}^2}{x_0}\sigma} = \sqrt{d}\sqrt{1 + \frac{\mathrm{d}}{x_0}\sigma} \tag{2.13}$$

The diffusion contribution ($\sqrt{d}\sigma$) is still present but now the spread introduces a new term. The spread alone would introduce a linear dependence on the drifting distance that for large distance will dominate on the square root diffusion term.

2.6.2 Example of Diverging Radial Flow

One of the rare detector that presents a diverging flow is the GEM detector. As shown in Fig. 2.9, the GEM field can be considered locally radial in the region between the hole centre and the walls. In the real case the velocity is decreasing going away from the center that is just the opposite of what we developed in the previous paragraph. Thus in this example we treat again the case of a toy model only using, for the parameters, values that can even be applicable to a GEM

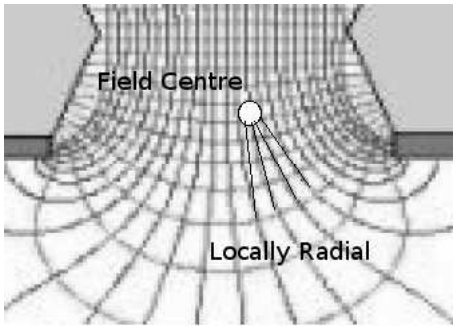

Figure 2.9: GEM field as seen locally radial

In this case the values of the parameters will be: x_0, the distance between the centre of the cloud and the field centre, equal to 10 μm, the diffusion coefficient in a standard gas

like Ar 70% / CO_2 30% is $\sigma = 200$ μm over 1 cm drift and the maximum value of the drift distance d = 20 μm.

Fig 2.10 illustrates what happens:

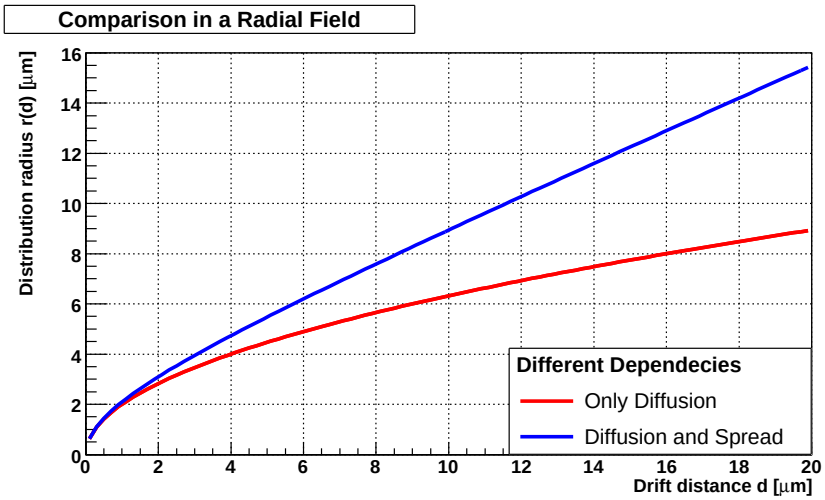

Figure 2.10: Distribution Radius changing considering only one effect or both effects

The blue curve has a dependency very similar to the diffusion for small distances but at large distances it becomes linear: it means that the diffusion plays an important role at the beginning but in the end the spread induced by the non-homogeneous electric field will dominate. If one considers only consider the diffusion a factor 2 mistake would be made: after 20 μm simply the diffusion term would give a spread of around 9 μm, while the combination of the two effect a spread around 15 μm. The conclusion is that this effect is very visible in a diverging field configuration. Considering also the effects induced by the drift-spread will help in calculating better some relevant parameters in a simulation like the losses on the wall, the particles drift path and the gain.

2.6.3 Two Dimensional Converging Radial Flow

We decided to develop a toy model also for this case. It was treated as the diverging one but considering steps of decreasing δ instead of increasing. The dependence of the radius enlargement on the drift distance in this case will be

$$r(d) = \sqrt{d}\sqrt{1 + \frac{x_0 - d}{d}}\sigma \tag{2.14}$$

The real case of a converging radial field (such as the one of a single wire chamber) will have the velocity increasing going towards the centre, while in this case it is again reversed. As parameter we decided to use some values that can be similar to the ones in a ATLAS Drift Tube (DT). In addition the transverse diffusion, considered in this model, is not present in the ATLAS real case. Thus we choose $x_0 = 1.5$ mm, $\sigma = 200/\sqrt{(3)}$ μm over 1 cm and d represents a variable going towards the centre of the field, Fig 2.11 shows the results.

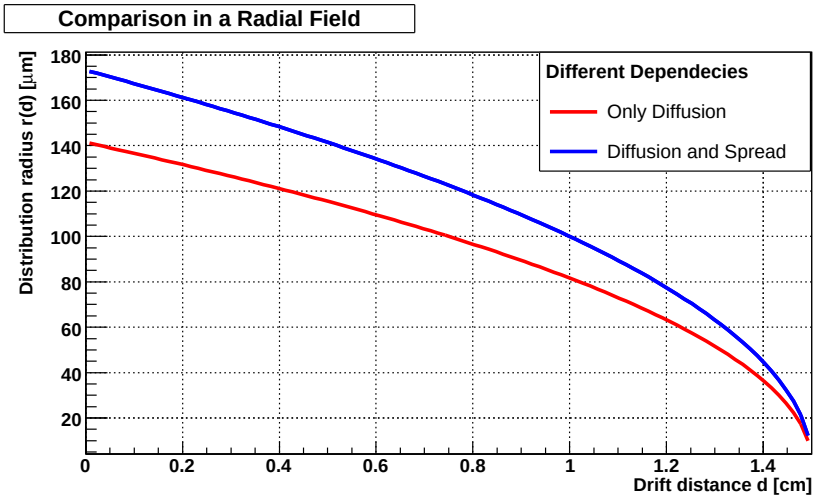

Figure 2.11: Distribution Radius changing considering only one effect or both effects. The cloud starts at 1.5 mm and moves back to zero

The starting radius is considered at $d = 1.5$ mm and the distribution spreads going towards the centre. Considering both effects will give in the end a radius around 170 μm while the single diffusion would give a value of about 140 μm: the effect is smaller than the previous case but the diffusion alone takes into account a factor 1.25 less.

Chapter 3

Gaseous Detector

3.1 Different Operation Regimes

The different gaseous detectors can be characterized by different factors: the voltage applied, the gain and the capability of measuring the energy of the particle. Based on this features it is possible to divide the detectors in four areas: the ionization chamber, the proportional chamber, the Geiger-Mueller detector and the streamer chamber. Figure 3.1 shows the different operating regions.

3.1.1 Ionization Chamber

This is the simplest gas detector and it is based on the idea of simply collect the charges created by an interacting particle without multiplying them. The resulting positive ion and free electron are the basic constituent of the electrical signal. Of the many types of collision that will normally take place between free electrons, ions and neutral gas molecules the most important are: 1) **charge transfer**: an electron is transferred from a neutral molecule to an ion, reversing the two initial states; 2) **Electron attachment**: a free electron is kept by a neutral molecule that becomes a negative ion; 3)**Recombination**: an electron is absorbed by a positive ion, giving rise to neutral molecule. As described before the collision of electrons with many atoms can also result in diffusion. In the Ionization Chamber to be able to acquire a signal, it is necessary in particular to avoid recombination; to reach this result, a sufficiently large electric field has to be applied which give rise to the movement of the electrons and to the so called *Ionization Current*. This field has to be large enough to collect charge.

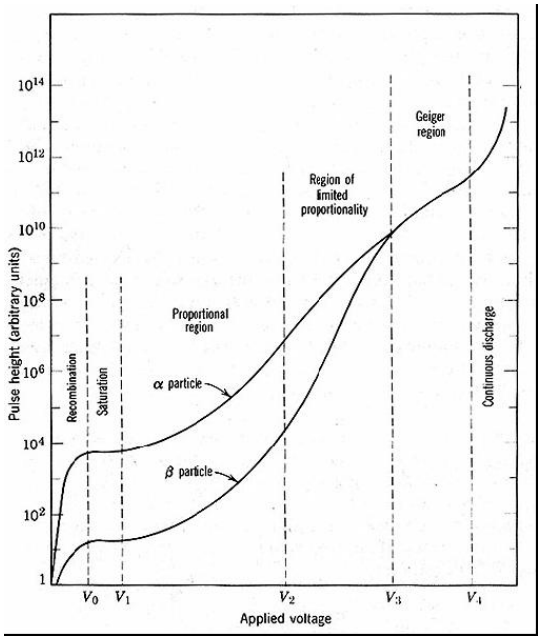

Figure 3.1: Gas detectors gain dependence on the voltage applied, [Kno99]

3.1.2 Proportional Chamber

The proportional chamber is a gaseous detector that rely on the phenomenon of gas multiplication to amplify the charge represented by the original electrons created within the gas.

Gas Multiplication is a consequence of the increasing of the applied electric field to sufficiently high value. Free electrons are easily accelerated by the applied field and may have significant kinetic energy when undergoing a collision. If this energy is greater than the ionization energy of the neutral gas molecule, it is possible for an additional ion pair to be created in the collision. Because the average energy of the electron between collisions increases with increasing electric field, there is a threshold value of the field above which this secondary ionization will occur. In typical gases, at atmospheric pressure, the threshold field is around 10 KV/cm. The new electrons created are accelerated too by the field and can give rise to others pairs. The gas multiplication process takes the form of a cascade, known as the *Townsend Avalanche*. The equation ruling this process is the so called Townsend Equation:

$$dn = n \cdot \alpha dx \tag{3.1}$$

where n is the number of electrons, dn is the new number that will be created and α is the *First Townsend Coefficient*. This coefficient is simple the inverse of the mean free path for

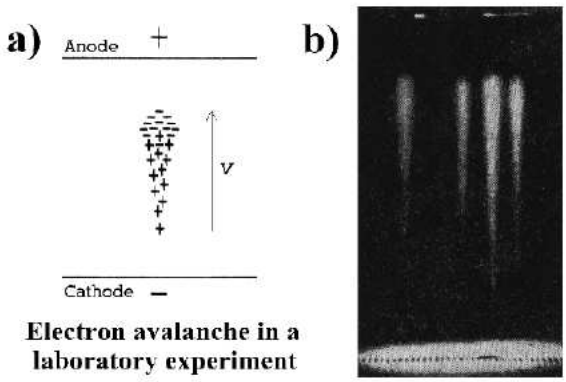

Figure 3.2: Typical Avalanche Shape, [Sta00]

ionization of the electron in a certain gas mixture, and is obviously dependent on the specific gas mixture. In addition, the first Townsend coefficient is a strongly-depending function of the reduced electric field E/p where p is the pressure. Therefore it will depend strongly on the position in a non-uniform electric field. The most general way to solve 3.1 is

$$M = \frac{n}{n_0} exp(\int_{x_1}^{x_2} \alpha(x)dx) \tag{3.2}$$

where M represents the multiplication factor, starting with n_0 pairs. The typical drop shape of an avalanche is shown is Fig 3.2.

Using this multiplication phenomena, the pulses generated are higher than the ones created in ionization chambers and this kind of detectors (operating in pulse mode) can be applied to situations in which the number of ion pairs generated by radiation is too small, for example for low energy X-radiation. With this kind of detector it is possible to measure the initial value of the energy of the interaction particle, because the amount of charges produced in the avalanche is still proportional to the pairs number created by the radiation

3.1.3 Geiger-Mueller Counter

If the value of the electric field is still increased we enter in a new region of operation. The Geiger Mueller counter has in common with proportional chamber the fact that they also employ the gas multiplication but with a substantial difference: in proportional chambers each original electron leads to an avalanche that is basically independent from all the other avalanches; in Geiger-Mueller tubes, at very high electric field, one avalanche can itself trigger a second avalanche at a different position in the chamber. This process becomes suddenly

divergent and an exponentially growing number of avalanche can be reached in a very short time. Once this *Geiger Discharge* reaches a certain size, however, collective effects of all the individual avalanches come into play and ultimately terminate the chain reaction. Because this limiting point is always reached after about the same number of avalanches have been created, all pulses from a Geiger tube are of the same amplitude regardless of the number of original ion pairs that initiates the process. Therefore a Geiger detector can only be used as a simple counter.

3.1.4 Streamer Mode

Pushing again the value of electric field we enter in an other regions in which streamers are formed. At very high electric field it is possible to generate, from the first avalanche other photon-mediated avalanche that can sum to the first one giving rise to the formation of the streamer. This kind of phenomenon has been used in detectors like RPC. This breakdown region is reached if the Raether limit has been overcame:

$$\alpha \cdot x \simeq 20 \tag{3.3}$$

or equivalently if the gain M is around 10^8

3.2 Brief History of Gaseous Detectors

3.2.1 Multi-Wire Proportional Chambers

Invented in 1968 by G. Charpak *et al*, this detector represents an important revolution in the particle detectors field. For his invention Charpak was awarded the 1992 Nobel-Prize in physics . Thanks to its high-rate capability and millimiter precision, this detector quickly replaced bubble and spark chambers: with an appropriate electronic read-out a MWPC was 1000-fold faster than the existing techniques. A multiwire proportional chamber consists essentially of a set of thin, parallel and equally spaced anode wires, symmetrically sandwiched between two cathode planes. When a negative potential is applied to the cathodes, the anodes being grounded, an electric field is created. A particle passing in the detector volume leaves a trace of ions and electrons: the latter ones drift towards the nearest anode wire and, as in proportional counters, are multiplied near it where the electric field is very high. Instead the ions drift toward the cathode planes where they are collected. The improvement respect

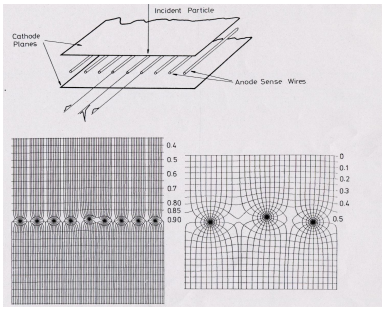

Figure 3.3: Schematic view of a MWPC and its equipotential lines, [Sau77]

to previous technology is evident: with MWPC was possible to determine the position of an incoming particle using only one detectors instead of using arrays of proportional counters. Several variations of the initial design have been developed over the years to maintain this detector still competitive; in fact today MWPC are still important components of many particle-physics detectors. Nevertheless, with higher demands of High Energy Physics (HEP) the limitations of this detector became evident. For example the spatial resolution is limited to the possibility to place and hold the thin anode wires not closer then few mm and there was a limited wire length above which instability arise due to electrostatic repulsion. The last and maybe more important problem is the production of positive ions that gave rise to the space charge effect and consequently to a rate capability limitation. Figure 3.3 reports a general scheme of this detector.

3.2.2 Micro-Strip Gas Chambers (MSGC)

In 1988 A. Oed invented a new kind of gaseous detector: the Micro-Strip Gas Chamber. This detector does not contain wires but uses very narrowly spaced conductor strips laid on a insulator support. Alternatively the strips are supplied with different voltages: for example it is possible to ground the anode strips and put negative voltrage on the cathode strips as well as to the drift plane. The high electric field necessary to create avalanches is created between near strips. With this kind of detector it was possible to increase the spatial resolution (the strips are at a small distance respect to the wires) and reduce the space charge effect because the ions are quickly collected by the nearest cathode strips. Fig 3.4 shows this detector.

This detectors show their problems on long-term operation. Imperfections in the detector or unusually large deposit of energy can cause discharges that can damage the strips or even

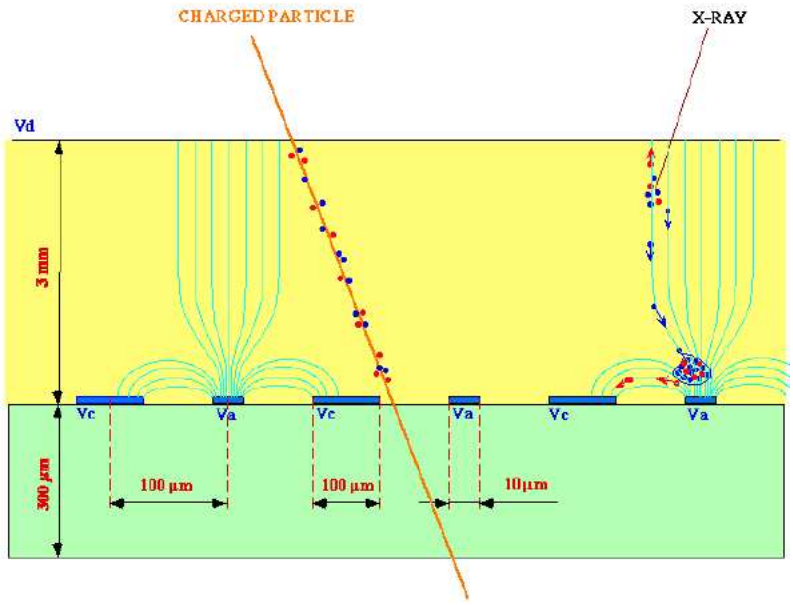

Figure 3.4: Schematic view of a Microstrip Gas Chamber, [Eve06]

produce short circuits in the detector. Another problem was the high rate of ageing, that is the loss of performance during a long period of sustained irradiation.The permanet damage was attributed to the creation of polymers in the avalanche that stick to the electrodes or to the insulator causing discharges and disturbing the counting process. The creation of these polymers can be due to different factors like the Gas, the Gas System, the MSGC support or the construction material. A careful choice of the previous factors can lower the not-wanted effects.

3.2.3 Micro Pattern Gas Detectors

The need of higher rate capability leads to the investigation of new techniques to create detector such as photolithographic processes and small dimensions This gave origin to a new family of gas detector: **The Micro Pattern Gas Detectors**. Their name is due to the fact that the elementary cells are at least one order of magnitude smaller than the ones constituting previous detectors. Examples of this kind of detectors are Micro-Dot Avalanche Chamber, Micro-Groove Detector, MicroWire Detector, Micro Gap Chamber, ... Another very popular design is the MicroMegas, which consist of a very thin metal mesh stretched at a very small distance, 50 to 100 μm above the readout electrode. The very high field (30

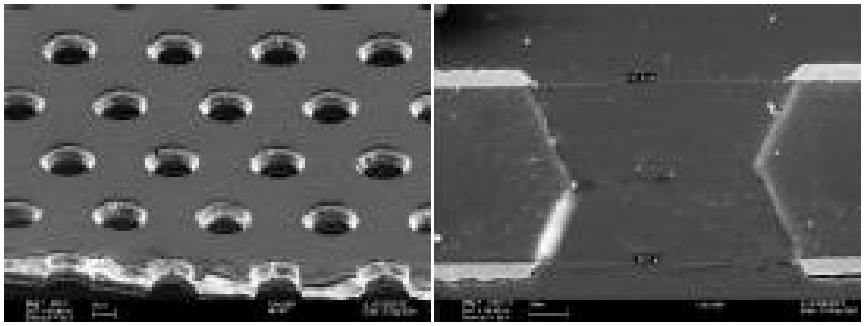

Figure 3.5: Microscopic view of the Gas Electron Multiplier

Kv/cm) over the gap multiplies the electrons. The Gas Electron Multiplier, the detector used for our research, belongs to this region and is one of the most advanced micro pattern detectors.

3.2.4 Gas Electron Multiplier (GEM)

Invented by Fabio Sauli in 1997, the Gas Electron Multiplier consist of a thin insulating ($\backsim$ 50μm) foil copper-clad on both sides and perforated by a high density, regular matrix of holes (typically around 100 per square millimeter). Typically the distance between holes (pitch) is 140 μm and diameters of about 70μm. The mesh is realized by conventional photolitographic methods as used for the fabrication of multi-layer board (see 3.5).

Upon application of a potential difference between the GEM electrodes, a high dipole field develops in the holes focusing the field lines between the drift electrode and the readout element. Electron drift along the channel and the charge is amplified by a factor that depends on the field density and the length of the channel (see 3.6). At the beginning GEMs were used only as preamplifier for MWPC or MSGC but nowadays GEMs are used as detectors themeselves, read out by strips or pads. GEMs still suffer from discharges, but this problem can be considerably reduced by cascading several GEMs so that each can be operated at lower voltages. A big advantage of GEMs detectors is the conservation of ionization pattern; thanks to this improvement the read-out system can be designed independently from GEM structure and suiting in the best possible way the aim of the experiment. The decoupling of the amplifying structure and the read out board is another one of the most important advantages of the GEMs. In addition GEMS have a natural property of suppressing ion feedback, making them very interesting for Time Projection Chamber (TPC) endcap.

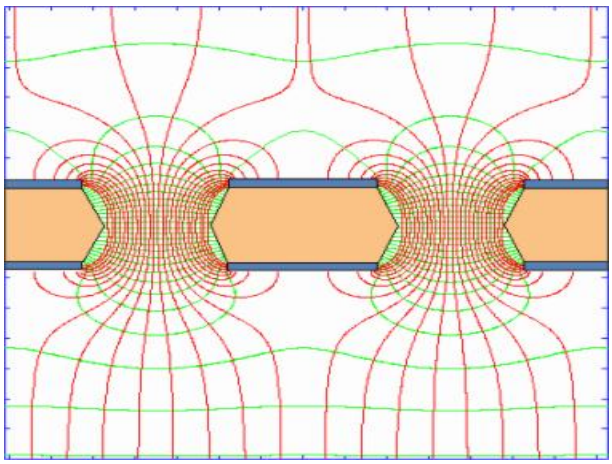

Figure 3.6: Drift and equipotential lines of a GEM detector

3.3 Uses of Gas Detectors

Compared to other kind of detectors, mainly the Solid-State detectors, the Gas Detectors have lower resolution. But the Solid-State detectors have also a much higher cost than the gaseous ones. In the high energy physics experiment, such as the Large Hadron Collider (LHC) experiments, the silicon detectors are used in regions near the collision point for reconstruction and tracking, but when it is necessary to cover large area, the gaseous detectors are used. The muon chambers, usually situated in the outer parts of the detector to cover large areas far from th beam pipe, are gaseous detectors for all major experiments Atlas, CMS, LHC-b and Alice.

3.3.1 Use of GEM in High Energy Physics

A HEP experiment that uses GEMs is COMPASS. In this fixed target experiment triple-GEM detectors are used in the small area tracker. The GEM technology is also used in the PHENIX upgrade at Brookhaven National Laboratory.

GEM detector are also used in the LHC experiment TOTEM. The aim of this last experiment is to measure the total proton-proton cross section. Ten triple GEM will be used for the telescope before and after CMS for tracking. LHC-b uses triple-GEM detectors in the innermost region of muon detectors because of the high beam intensity there. In the rest of the muon chamber MWPC are still used.

The main future employment of GEMs might be for the endcap of TPCs. The reduced

ion back flow together with increased robustness, fast signal and better two-track resolutions, seems to favour this kind of detectors in that use. Nevertheless the understanding of stability of gain of this detector at low rate is very important for any future TPC applications, especially for the ILC. This gain stability was studied throughtout this work.

3.3.2 Other GEM Application Fields

GEMs are also considered for use in different other fields, mainly in the medical one. In medical imaging the use of GEMS can reduce the amount of necessary radiation because GEMS are sensitive to single photons. Again in the medical field, the GEMs are under study to be used in an on-line control and verification device for cancer radiation treatment. In plasma diagnostic GEMs can be used because of their high rate capability. A photoelectric X-ray polarimeter for the study of neutron stars and black holes holes has also been developed. The GEM boron-coated to reveal neutron have been developed with promising results. The development of GEM photomultipliers are also under investigation. In this work we tried to develop a new GEM based-detector for applications in Positron Emission Tomography (PET) scanners.

More detailed informations about all these applications and new uses for GEM concept can be found at the website of CERN's Gas Detector Development (**GDD**) group: *http://gdd.web.cern.ch/GDD*.

Chapter 4

Manufacturing and Description of a GEM-based detector

4.1 Production of GEMs

The Gas Electron Multiplier consist of a very thin, two-side metal-clad polymer foil perforated with a high density of photolithographically etched holes. The production process was developed by the CERN surface treatment Service (R. De Olivera, A. Gandi and L. Mastrostefano). The basic material for the production process is a 50 μ thick kapton foil with two layers of metal (mainly copper) on the opposite sides. It is possible to identify some important steps in the production of a GEM foil.

1. The surface of the raw foil has to be cleaned before starting the production
2. Two identical masks with the desired pattern are realized on a film
3. The masks are optically aligned with an accuracy around 5 μm
4. The foil is coated with photoresistive layer, and inserted between the two masks
5. The structure is exposed to UV-light, so that the copper hole pattern is engraved on the photoresist on both sides of the sheet
6. A conventional sequence of solvent and acid baths is used to etch the metal, liberating the holes
7. Then the Kapton layer is dissolved using chemical etching. The pattern in the metal layer serves as a mask and the holes are dug from both sides producing the characteristic

double-conical shape. The technique used for the etching is the ChemicalVia technique. This chemical technique of making microvias was also developed at CERN and consist of three different chemical baths (Na_2CO_3, $FeCl_3$, and ethylene-diamine bath). With chemical etching it is possible to make any pattern of small diameter holes in a cheap and fast way. The process always takes 10-15 minutes, independently of the number of holes desired since all the holes can be formed in the same chemical bath.

8. After masking the hole area, the superfluous metal on edges is etched away, leaving a narrow frame with just kapton around the structure.

9. To clean the foil from all aggressive liquids, it is washed in four different baths: floating water, denionized water, demineralized water and alcohol. Afterwards the foil is dried in air at 80 degrees Celsius

10. A first test is performed with an ohmmeter in air: in this test the resistivity between the two GEM side has to exceed 3 $G\Omega$

11. The GEM foils are packed individually into dust free cotton sheets and a protecting mylar envelope.

All the phases described above are represented in a more schematic way in Fig 4.1

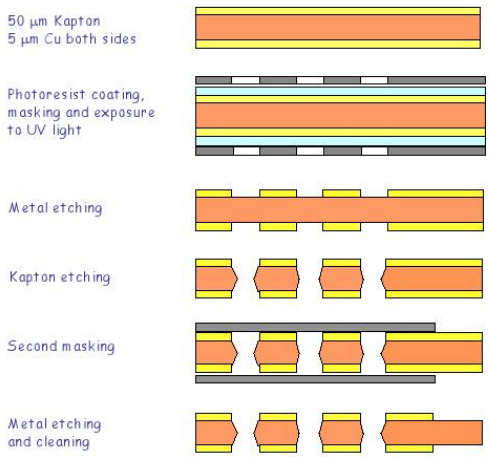

Figure 4.1: General Scheme of GEM production process

The final results is a GEM foil with double-conical holes with typical measure of 70 μm copper diameter, 50 μm kapton hole center diameter and 140 mum pitch.

At the moment the main production of GEM is at CERN but, owing to the higher request, the TT-CERN department is trying to find external factories that can produce GEMs in industrial way and at a even lower cost.

4.2 GEMs: From production to use

The PCB workshop delivers flexible GEM foils. To be able to use them, it is necessary to create a support that allows the GEMs to be put in a working setup. The foils need are mounted on frames of different dimensions (from 5 cm X 5 cm to 10 cm X 10 cm in our case. A raw GEM foil is therefore softly stretched by two Plexiglas frames. This stack is then placed into an oven and gently heated to 40 degrees Celsius: the thermal expansion extends the foil uniformly. Epoxy is then spread over two fiberglass frames placed on top and bottom of the GEM foil. The stack is put in the oven again for the time necessary for the epoxy to harden. After removing the support and cutting away the excess kapton, the framed GEM is ready to be mounted in a detector.

Always, before and after framing, each GEM foil is checked in clean room for discharges and too high leakage currents. First of all, the foils are flushed with nitrogen gas to remove the majority of dust particles. Then a voltage applied between electrodes through a high value protection resistor is gradually increased up to 500 V. If this operation provokes either a discharge or a leakage current higher than 5 nA, the GEMs are discarded. Some foils can be recovered with the following procedure:

1. The GEM foil is flushed again for a longer period with the cleaning nitrogen gas. This step can be repeated several times before having effect, especially if the behaviour shows improvements each time.

2. If inside the GEM foil a big short-circuit is present, this can prevent reaching the maximum voltage. Connecting the foil to a low-voltage power supply with a high current setting (several hundreds micro Amperes) can sometimes burn the impurity responsible for the short and recover the foil.

3. If the GEM is still not behaving properly, the foil is returned to the PCB workshop where it will be again cleaned in chemical baths.

4. If none of the methods above works, the GEM foil is not used anymore.

If a GEM foil can keep without problems 500 V, then the electrical contacts are created and it is placed in the mechanical support that will be used in the laboratory. After having connected the external protections resistors in this support, the GEM is again flushed with nitrogen and tested putting one GEM side to ground and the other to 500 V. If also this final check is OK, the GEM is ready to be used in a detector.

4.3 General Description of our standard experimental setup

4.3.1 The Detector

Because of the need of high flexibility and interchangeability, all the measurements were performed using a special designed research detector. Figure 4.2 show the visual description of such a detector and Figure 4.3 the external view. The basic setup allows many and flexible changes in number and type of GEMs foils as well as in the distances between the different electrodes (drift, readout and GEMs). The read-out structure is placed on a fiberglass backplane and provided with electrical contact to allow the acquisition of the signals.The fiberglass plane serves also as support for the high voltage connections. A second fiberglass frame is glued on this plane and includes the gas inlet; the gas outlet is hosted in a third fiberglass frame, that also mounts kapton or mylar window that allows the radiation to enter the detector. The frames are assembled with metal screws; a special rubber O-ring, put between the two frames, provides the gas tightness. The detector is put always under the gas flow and two flow meters, one on the input and the other on the output, control if the flux is the same after and before the detector. If this is not the case, it means that there is a leakage that must be fixed.

Inside this support four holes at the four corners are drilled at distances needed for the specific scope. Four Teflon screws are screwed in this four holes. GEM foils (shown in Fig 4.4), and the drift cathode (usually a full metal-kapton sheet), mounted on square frame with four holes in the corners, are inserted in the four pillars and kept at the correct distance using insulating spacers of thickness from 0.5 mm to 3.5 mm. These spacers together with the electrodes frame (usually 0.5 mm or 1 mm thick) define the distances between the different electrodes.

The whole chamber is then mounted on a metal support fixed to an optical bench rail that allows the chamber to be moved in the three directions and rotated.

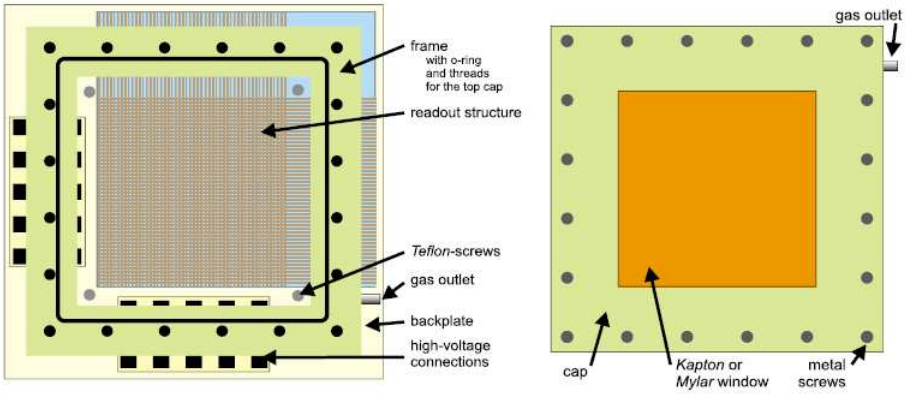

Figure 4.2: Schematic view of the special research detector, [Eve06]

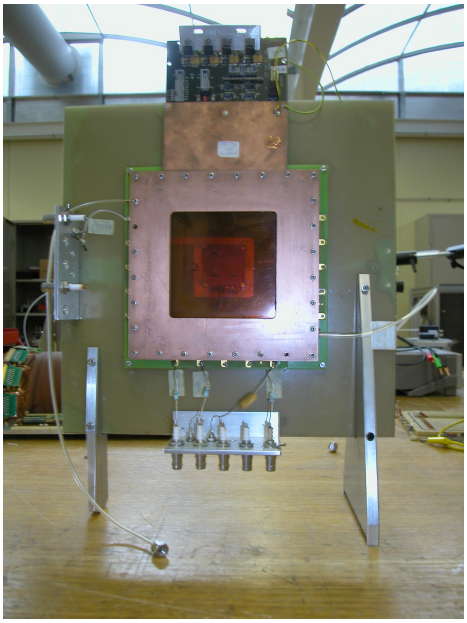

Figure 4.3: External view of the research detector

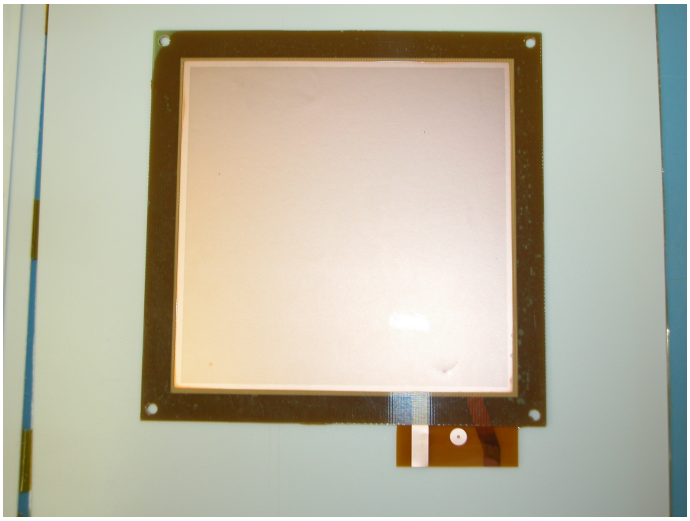

Figure 4.4: A standard GEM foil

4.3.2 Radiation Sources

The main source used in our experiments was a collimated beam of soft X-Rays. The X-rays tube has a Cu-Target and thus the X-Rays produced have an energy of 8.9 KeV. The profile of the beam is gaussian and the X-rays are sent to the detector using different opening collimators. The generator is mounted on the optical bench, allowing it to be moved in different directions, depending on to the specific necessity. The intensity of the beam can be chosen changing the filament current in a range from 0.04 mA to 4 mA. Even with the filament current at the lowest value, the flux is rather high. To further reduce the rate, two copper attenuators can be mounted directly on the exit of the collimator. A remotely activated shutter, placed in front of the beam, allows to stop the irradiation. Also radioactive sources were used: ^{55}Fe yielding X-Rays of 5.9 KeV and a ^{90}Sr beta-emitter with very high activity.

4.3.3 High Voltage supply

The high voltage can be supplied to the detector in two different ways: using a voltage divider or with separate power. The voltage divider is safer for the GEMs, because in case of discharge there is a global decrease of the voltage, avoiding the possibility of getting too high electric field in the detector. An example of this kind of potential distribution for triple GEM is shown in Fig 4.5. Using individual power supplies it is mandatory to install between

the HV contact and the electrodes contact a 1 MΩ resistor; in case of discharge this resistor reduces the potential applied faster than the current limit in the power supply. This second operating way can result in irreversible damages to the foils, but sometimes it is necessary to follow this way because it allows to easily modify easily the operating voltages of the detector. In the case of resistor divider the power supply used was CAEN N470, while in the other case several CAEN N471A HV Power Supply were used.

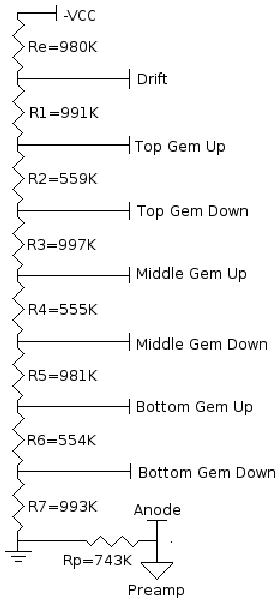

Figure 4.5: HV supply using a resistor divider for triple GEM detector

4.3.4 Gas System

The gas mixture used in all the measurements was a mixture of noble gas and quencher. The choice was always a mixture of Argon (Ar) and Carbon-Dioxide (CO_2) in different percentages. Mixtures like this are relatively cheap, non-toxic and non-flammable. Part of the measurements was performed using a complete gas mixing system in which it is possible to vary the relative amount of the two gases, while the other part was done using premixed bottle. The flow used was always around 5 l/h.

4.3.5 Data Acquisition System

The signal coming form the detector was preamplified using ORTEC or CAEN preamplifier and then amplified using a research amplifier (always, ORTEC or Caen). Then the signal was

analyzed using NIM modular electronic and recorded using the CAMAC system (CAMAC Controller 116A and LeCroy Charge ADCs). The CAMAC was connected to a computer where the data were stored. In this computer there was also an acquisition program which gives the commands to the CAMAC architecture.

4.4 General Description of a GEM-Based Detector

The GEM detectors are gaseous detectors belonging to the proportional family. As explained before, this device consists of a thin polymer foil, metal coated on each side and perforated by a high density of holes. Each hole works as an individual proportional amplifier. GEM foils inserted in a configuration containing a drift electrode and a read-out pattern forms the GEM based detector.

The electrons created in the drift region (the region between the drift electrode and the first GEM foil), are driven by the drift electric field in the GEM holes. Then, in case of multiple structures, they go to the second GEM foil, drifted by the transfer field and finally reach the readout structure passing through the induction region. On approaching the GEM hole, and starting from a critical value of field, electrons begin to multiply in an avalanche that increases exponentially along the channel. In absence of spreading effects, electrons and ions remain confined to the central region of the channel and are transmitted through the structure. Experimental results show that a field dependent fraction of the electron charge is actually collected by the bottom GEM electrode.

The real gain of a GEM (or multiple GEMS) is defined as the ratio of the number of electron yielded by the amplification structure to the ones coming from primary ionization. Due to dispersive effect the Effective Gain of a GEM, the one measured by a read-out anode, generally smaller than the Real one. Increasing exponentially with the applied voltage on the GEM, the effective gain depends on geometry (holes diameter and pitch), externals fields and Gas mixture used. For the $Ar/C0_2$ mixtures (the ones always used in our studies) Figure 4.6 reports the Effective Gain versus the GEM applied voltage: it is obvious that with higher percentage of Ar the voltage needed to reach higher gain is lower.

With smaller hole diameter, it is possible to reach higher real gain, but the effective gain actually reaches a saturation plateau around a value of 70 μm (see Figure.4.7). This is a very important feature because this saturation helps to relax the tolerance requirements on the hole diameter, a particular important feature in view of manufacturing large areas detectors.

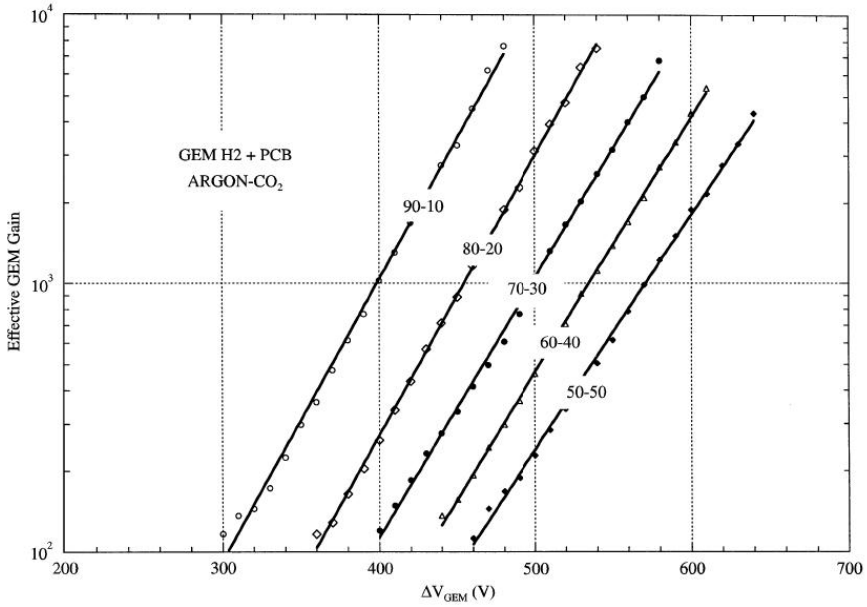

Figure 4.6: Effective GEM gain as a function of voltage for different concentrations of $Ar - CO_2$, [BBCG$^+$98]

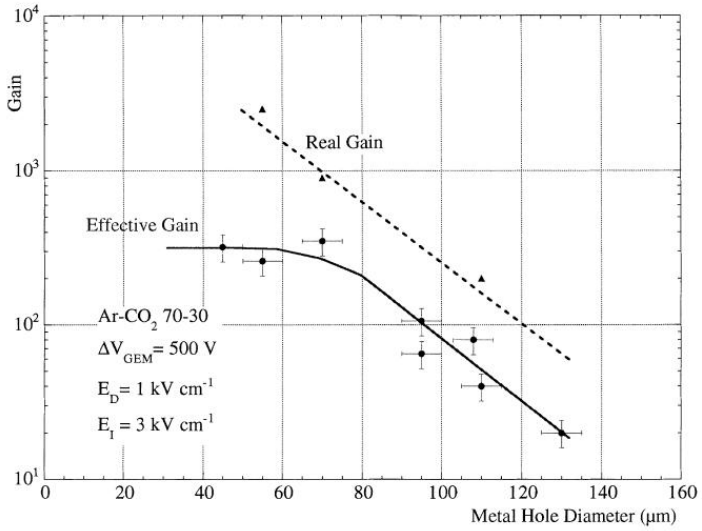

Figure 4.7: Effective and real gain as a function of hole diameters, [BBR$^+$99]

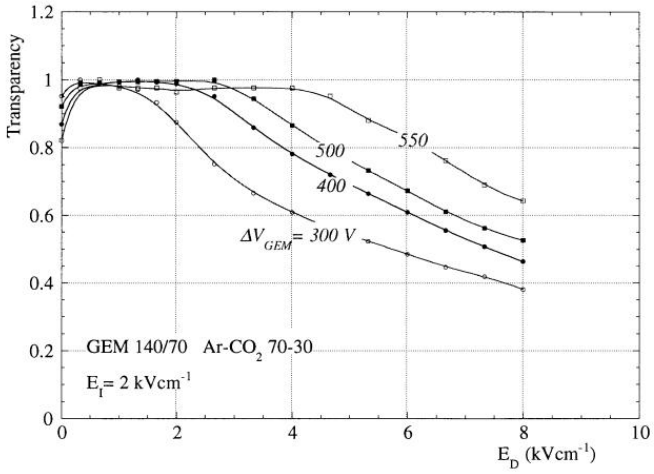

Figure 4.8: Electron collection efficiency (transparency) as a function of drift field for several values of GEM voltage and low induction field, [BBR+99]

The external fields, drift,transfer and induction ones, play a very important role in defining the electrical transparency of a GEM foil. The drift lines of a GEM foil are shown in figure (3.6). Depending on the strength of the drift field, the field lines go through the holes or terminate on the copper layer; for a fixed GEM voltage and suitable induction field, the electrical transparency increases, when the drift field is enhanced. At a certain value a plateau is reached; from Figure 4.8 it can be seen that this value is between 1 and 2 kV/cm. At too high drift fields a certain fraction of the electrons terminate on the GEM electrode.

The induction field affects the charge collection to the read-out electrode. At high induction field less electrons will end up at the lower face of the GEM and more will reach the anode. In Ar/CO_2 based mixture, parallel plate multiplication begins in the induction region above 8 kV/cm with a consequent fast increase of the gain; this mode of operation is unsafe because it may allow a discharge to propagate to the readout electrode. Figure 4.9 shows that for values between 2 and 4 kV/cm the effective gain almost does not depend on the induction field leaving more tolerance in choosing the other parameters of the detector.

All this behaviour can be simulated using the programs *MAXWELL*[1] and *GARFIELD*[2].

[1]MAXWELL, Ansoft Co., Pittsburg, PA, USA
[2]R. Veenhof

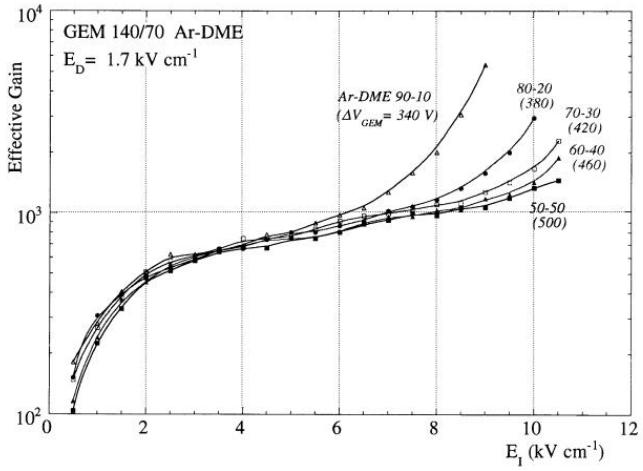

Figure 4.9: Effective Gain as a function of induction field in a range of gas mixtures and GEM voltages, [BBR+99]

4.4.1 Advantages of GEM detectors

Owing to the simple shape of the GEM foil there are many advantages in using this kind of detector. Being so thin and completely autonomous it is possible to create multi GEM structure putting in sequence two or more GEM foils. This multiple structure allows reaching higher gain with lower voltage on the individual GEM avoiding the possibility of a discharge. Figure 4.10 shows this behaviour. In addition, the GEM multiple structure (more than the single structure which is also quite good) have a very high rate capability because of the absence of the space charge effects. The ion feedback to the drift region is reduced because the ions produced by the lower foils are mostly collected by the upper ones.

As the multiplication structure is separated by few mm gap from the read-out electrode, discharges generated in the GEM have a negligible probability to reach the read-out electronics (often very expensive), and damage it; this read out structure can be designed with very high flexibility in the geometry: examples of read-out are hexaboard, strips, non cartesian strips, pads,.... that can be optimized following the need of different experiments. In addition the readout signal will be very fast because only the fast part of the signal (the electrons) is collected.

Since the elementary amplifier device is the GEM hole, it is possible to construct GEM detector with very high freedom of shape and dimesions: square (COMPASS), half circular (TOTEM), circular (MICE), Semi-Cylindrical (NA49-Future, See Fig 4.11)

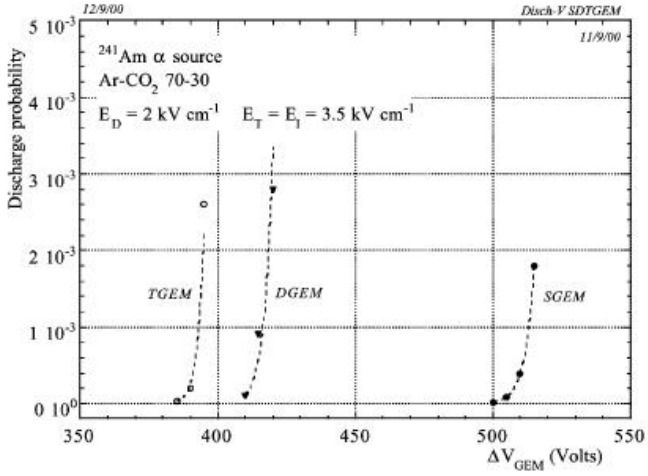

Figure 4.10: Discharges study for different structure, [BBCG+00]

Figure 4.11: From Left to Right: Three different kind of GEM detectors for three different HEP experiments: COMPASS,TOTEM and NA49 Future

.

Another very important feature is that this kind of detectors are completely insensitive to aging (see Chapter 5), the worsening of important detection parameters (loss of gain, resolution, ..) due to long-term, high radiation rate exposure.up to 100 mC/cm^2.

Chapter 5

Fundamental Characteristics of GEM detectors

After the general description of the Gas Electron Multiplier, it is important to explain the fundamental characteristic of this detector.

5.1 The Energy Spectrum

The process of detection in GEM devices, as all gaseous counter begins with the ionization of the gas. In Argon-based mixtures X-rays interact with the gas molecules through photoelectric absorption and, in the majority of cases, an Auger electron is emitted in the rearrangement of the excited gas molecules .The peak position in the Energy Spectrum is proportional to the energy deposited by the X-Rays and therefore it is possible to distinguish radiation with different energy. In addition to the absorption of all the photon energy there is a competitive process. If the energy of the X-Rays is greater than the threshold for an argon K-shell ionization (3.203 KeV) the photon may excite the atom giving rise to the emission of an X-Rays from the Ar-Kα or (less often) from the Ar-Kβ shells. If this Ar-Kα photon escapes from the detector, an amount of energy equal to the energy of the escaped Ar-X-Ray (around 2,9 KeV) is lost from the detector. There is a non negligible probability (15%) that this de-excitement photon escapes from the detector; in this case the amount of photon energy is lost. Initial X-rays will still create ion/electron pairs (through photoelectric absorption) but the number of such pairs will be less. In this case a pulse is still collected, but its energy is less than that of the incident photon by an amount equal to the energy of

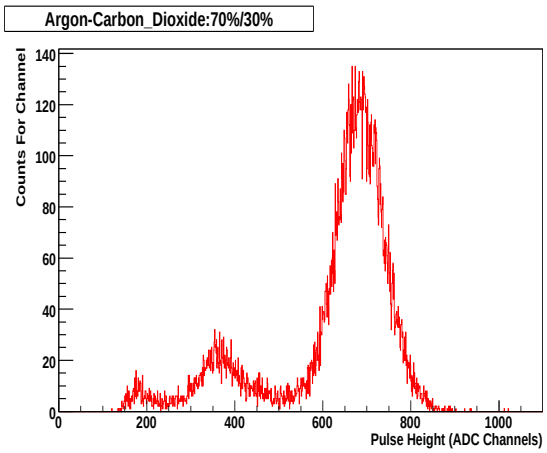

Figure 5.1: Gem Energy Spectrum acquired with Fe source, the lowest peak on the right is only noise

the Ar-Kα escaped photon. Therefore the typical spectrum shows two peaks: the first one is placed at the total energy deposited by the X-Rays (8.9 KeV for Cu and 5.9 KeV for Fe) and the second one, the Argon escape peak, is placed at an energy 3.2 KeV less (around 6 KeV for Cu and 3 KeV for Fe). Figure 5.1 shows a typical Energy Spectrum acquired with the ^{55}Fe source. The GEM energy resolution, defined as $\frac{FWHM}{PeakPosition}$ is around 20% at 5.9 KeV.

5.2 Discharges

The occurrence of discharges inside micro pattern detectors is one of the bigger operating problems. Due to the high electric field used for the amplification, there is the possibility to create discharges at certain sharp edges. These phenomena can be devastating for the detector and ruin the read-out electronics. It is fundamental to avoid as much as possible these discharges but because it is not possible to exclude them completely, the detector itself has to be able to support a small rate of breakdown.

Studies performed on GEM detectors revealed that they do not show any indications of deterioration after discharges. This can be explained by the fact that the hole geometry is not affected by them. In GEM detectors the readout is separated from the amplification region, protecting the electronics. But also in GEM some discharges can normally extend to the read-out anode and thus hit the electronics. This is the reason which special diode protection circuits are used for the amplifiers. These circuits are tested by provoking discharges

for example introducing strongly-ionizing particles, like alpha particles, in the detector and monitoring the frequency of discharges observed.

As explained in the previous chapter, it is possible to reduce the discharge probability by using multiple GEM structures. For example if a single GEM foil is used in standard mixture Ar-$C0_2$ with a voltage of 500 V a gain around 8000 is obtained (see Figure 4.6). In this case the discharge probability will be high. But if a Triple-GEM structure is used with each GEM gaining around 20, the same result is reached but with a lower discharge probability because the voltage difference on each single foil will is smaller. Figure 4.10 shows a plot of this effect.

5.3 Gain

As shown in Figure 4.6 the gain of GEMs depends on the gas mixture and applied voltage. Amplification sets in with a standard GEM around 250/300V potential difference on the two sides and then the increase is exponential. Knowledge of the voltage dependence of the detector gain is very important and it is fundamental to understand it very well. The gain measurement is always performed using the Copper X-Ray Generator. The effective Gain is measured for different interaction rate as:

$$G_{eff} = \frac{I_{ReadOut}}{n_{tot} \cdot F \cdot e} \tag{5.1}$$

where I is the current in Ampere measured on the readout anode, F the interaction flux, e the electronic unit charge and n_{tot} is the number of primary ionization pairs. At very high flux the pile up effect can lead to a not correct measurements of the interaction flux itself. To avoid this problem it is necessary to put a copper attenuator out of the collimator to work at lower rate. Knowing this attenuator factor it is possible to estimate correctly the real rate and thus the gain.

5.4 Rate Capability

The rate capability is defined as the the maximum flux before gain drops. A high rate capability is fundamental for application in High Energy Physics. Multiple studies have been performed with GEMs to understand their rate capability. It is important to remember that one of the reason to introduce the micropattern detectors was the low MWPC rate capability (around $10^4 Hz/mm^2$). It has been demonstrated that the GEMs does not show any decrease in gain up to $10^5 Hz/mm^2$. Figure 5.2 illustrates the GEM Rate Capability

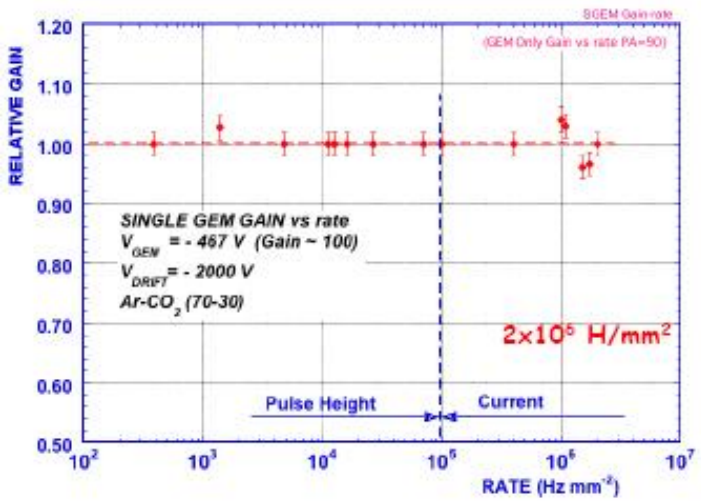

Figure 5.2: GEM Rate Capability: the gain does not suffer rate problems until $\sim 10^6$ Hz/mm^2, [Rop06]

5.5 Aging

Many studies were performed to check if the Gas Electron Multiplier is sensitive to aging phenomena. Aging usually leads to surface degradation of the electrodes and affects gain and rate capability of the detectors. In general, active species produced during the avalanche process can attach to the electrode surfaces. The main part of electrons and negatively charged polymers from the avalanches reach electrodes. Process of polymer film formation start in the regions with highest electric field strength. Electrons and ions can accumulate on the deposits, modifying the electric field and therefore the performances of the detector. Aging effect are local and start to show up only after a long period of irradiation. One of the main study shows that after a total collected charge of 20 mC/mm2, corresponding to seven years of operation in the worst case of the COMPASS environment, no loss of gain or of energy resolution is observed ([ADK$^+$01]). Other studies have extended the limit up to 100 mC/mm2. This demonstrates the relative insensitivity of GEM detectors to aging when operated with cleaned Ar-C0$_2$ mixture. Two reasons may explain this result: the fact that the gas amplification is localized inside GEM holes (far from electrodes and walls), and the small effect of possible polymerization deposits on the electric field in this region.

Chapter 6

Gain stability of GEM-based detectors

The gain stability is a very important parameter of gaseous detectors because any unwanted variation of gain can affect the energy resolution and cause a loss of efficiency. The studies performed are directed to better understand the roots of the processes that influence the gain variation. An inner outlook in this problems is necessary for use of GEMs in TPCs endcap for the future High Energy Physics experiments, in particular at the ILC.

6.1 TPC applications

A time projection chamber consists of a gas-filled chamber with gas detectors (nowadays the most used detectors are still the MWPCs) as endplates. Along its length, the chamber is divided into two halves by mean of a central high voltage electrode disc, which establishes an electric field between the center and the endplates. In addition a magnetic field is applied along the central axis of the detector, in order to determine the momentum of particles and to minimize the diffusion of electrons coming from ionization of the gas. The passage of a charged particle in the gas volume will produce primary ionization along its track. The z-coordinate (the one along the central axis of the cylinder), is determined by measuring the drift time from the ionization event to the endcap MWPC, in the same way as in a drift chamber. The other two coordinates are measured using the MWC detectors endcap: one coordinate (for example the x) is given by the number of hit wire; the other (the y) is measured along the wire direction and needs the use of cathode pads for the its determination.

The TPCs 3D localization is extremely useful in tracking charged particles in a high-track-density environment, and for identifying particles through their energy loss due to ionization ($\mathrm{d}E/\mathrm{d}x$)

6.2 Why to use a GEM endcap

In conventional TPCs the end-cap consists of multiwire-chambers. This type of detector provided good energy and spatial resolution for most of the experiments until now, but the next generation of detectors, such as the ones that will be installed in advanced linear colliders like the ILC, has to perform better in both aspects.

One of the major problem of the multiwire endcap is the $E \times B$ distortion that take place in the last millimeters of the drift regions where the drift electric field get superimposed to the radial electric field of the anode, creating a region of non-parallel electric and magnetic fields. In strong magnetic fields this distortion provokes a broadening of the electron cloud and a worsening of the resolution.

Another problem of the traditional multiwire endcap is the very high ion feedback. The ions created near the wire drift away with an initially high drift velocity. They can build up in the drift volume a large space-charge that can change the electric field and thus the drift proprierties of the following track that will not be reconstructed in the correct way. In addition the ions can add a slow part to the signal when living the high electric field region.

GEMs TPCs are able to overcame many of these shortcomings. As described before, in multiple GEM structures the majority of the ions is collected by the various electrodes, and typically only a few percent or less reach the drift volume. In addition, GEMs allow the use of easier mechanics and the robustness of the detector is increased because no wires need to be mounted.

A very important request that GEMs have to satisfy is the temporal and rate stability of the gain.

The temporal stability of the gain is necessary because a gain variation can affect the correct measurement of $\mathrm{d}E/\mathrm{d}x$. In a TPC the interaction rate is higher in the central part of the drift volume than in the outer part. The rate stability is important to guarantee the response uniformity throughout the detection volume.

One of the subject of this report is the study of the temporal response of gain of GEM based detectors.

6.3 Previous temporal stability measurements

Plot 6.1 shows the evolution of normalized gain with time and rate of irradiation and illustrates the results of precedent temporal stability studies. The GEM gain stability (timewise and spacewise) is around **20**%. All the studies described in this report deals with **smaller** gain modification.

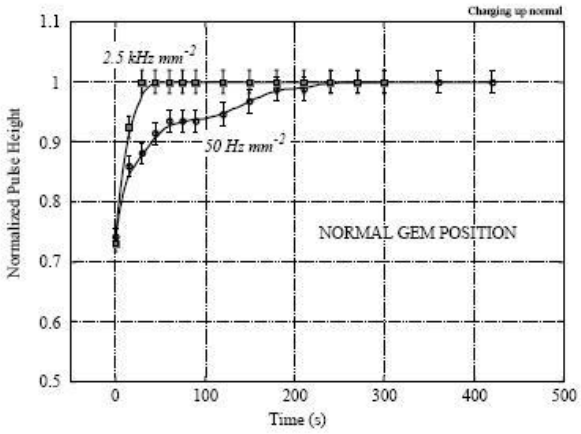

Figure 6.1: Previous studies of the temporal stability for COMPASS GEMs. The variation of the gain is present only in the first 200 seconds, [KAD+01]

6.4 Experimental Setup and Measurements description

The GEM foils used for this experiment are standard ones. The active area is small (3cm x 3cm area) and the detector structure is the one described in Chapter 4. The GEM were powered with 500V potential difference. The gas mixture used through all the measurements was Ar/CO_2 70%/30% and the radiation source the Cu x-Rays generator (8.9 KeV x-Rays). The collimated x-Rays source was used to be able to easily change the interaction rate and illuminate only a selected part of the detector. Both kind of HV power supply modes were used. Single and triple GEM structure were tested to understand if they have the same behaviour.

6.5 Possible Sources of Instability

At the moment three effects that can influence the modification of gain have been identified:

1. The movement of the charges within the kapton after applying the voltage on GEM sides (conventionally named polarization).

2. The charges produced in the gas that can attach to the kapton walls (charging up).

3. The direct photons conversion in solid materials (kapton or copper)

.

The last two effects are called *radiation effects*. The consequences of the polarization and of the radiation effects effects are qualitatively shown in Fig 6.2. In general the movement of charges inside the capton results in a gain increase while radiation effects in a gain decrease

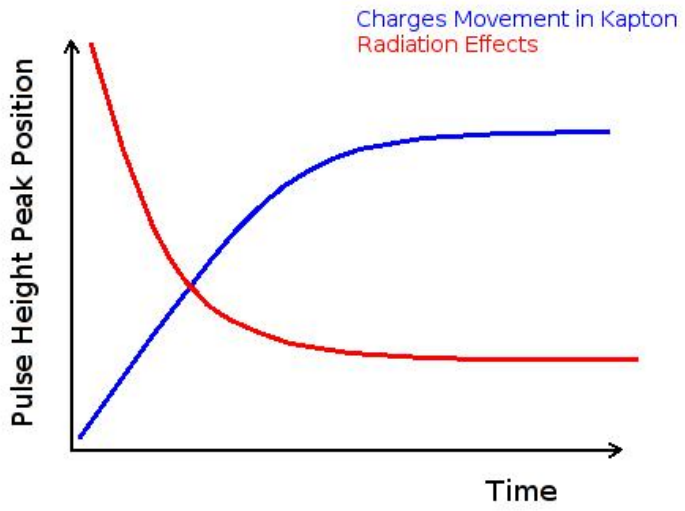

Figure 6.2: Graphical view of the consequences of the three effects

6.6 Measurements

To understand one by one the three effects different types of measurements were performed.

1. *SAME TIME MEASUREMENTS*: apply high voltage to all the electrodes and start to irradiate the chamber immediately.

2. *VERY LOW RATE MEASUREMENTS*: as SAME TIME but the chamber is irradiated only every 5 minutes for the minimum time needed to acquire a pulse height spectrum. The interaction rate is around few herts.

3. *ON BEFORE MEASUREMENTS*: apply high voltage to the chamber some hours before starting the irradiation

4. *POSITION SCANS*: acquire the spectrum in a long time irradiated point; move the x-ray source and acquire spectrum in neighbouring points

6.7 Single GEM Analysis

The effect of charge movement inside the kapton (the kapton polarization), was analyzed performing many *same time measurements* at different rates and some *very low rate measurements*. This last kind of measurement should give the possibility to completely disentangle the polarization effect from the radiation effects. The result of this analysis is shown in plot 6.3

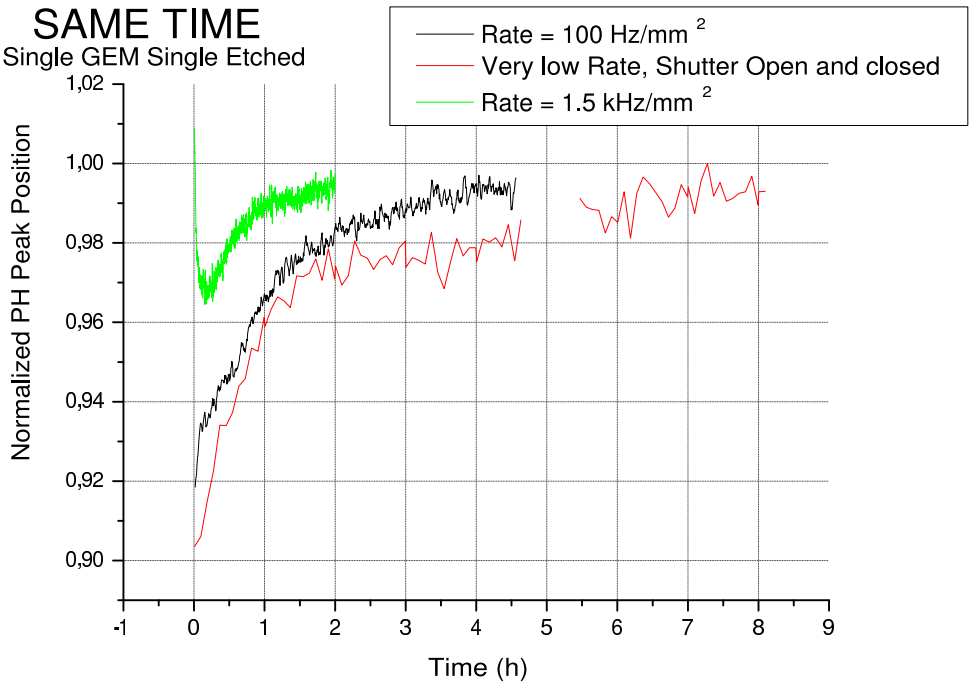

Figure 6.3: The effect of the kapton polarization: for low rate and very low rate only a gain increase is present while for high rate the gain increase follow an initial gain decrease

The low rate and very low rate measurements have more or less the same behaviour and seem to stabilize on a plateau after 10 hours. The high rate measurement show an initial

decrease because at the beginning the effect of the polarization is lower; after less than 10 minutes the kapton polarization takes over the radiation effects and the gain starts to increase. The three curves seem to stabilize on the same equilibrium line. The three different rates measurements were performed in three different moments and irradiating different points of the detector. All the variations are less than 10%. It is important to underline that the effect of charges movement inside the kapton is a global effect, it means that it interests all the GEM area while the radiations effects are local ones affecting only the behaviour of the irradiated points.

The position scan performed after the same time measurement at 100 Hz/mm^2 (Fig 6.4) confirmed these assumptions.

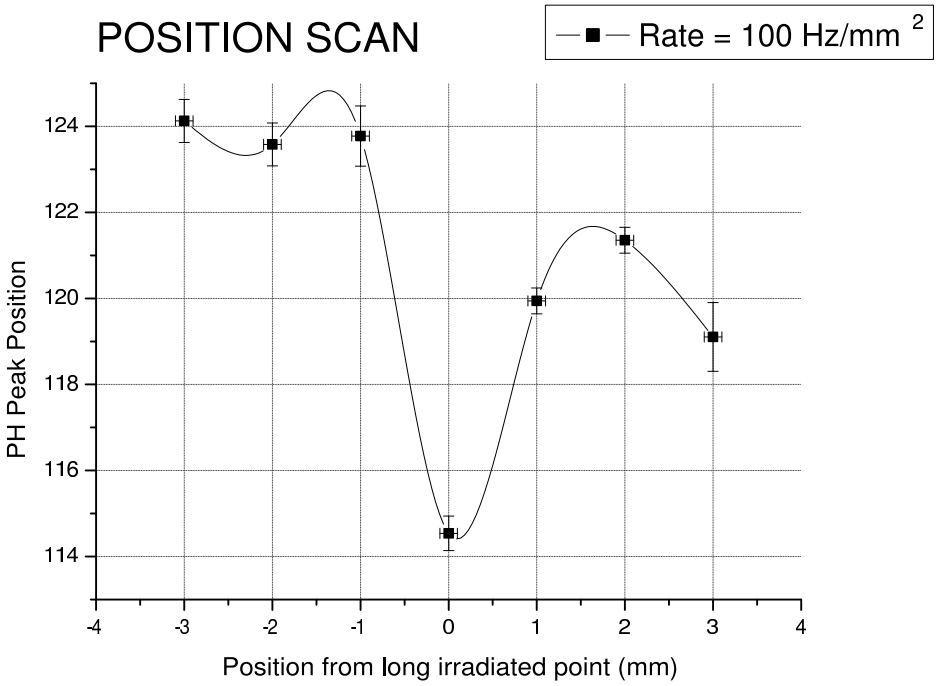

Figure 6.4: The long time irradiated point shows a gain decrease while the neighboring points do not; the gain increase due to kapton polarization interest all the GEM area while the gain decrease only the irradiated point (the minus sign is a convention for the the leftside points respect to the irradiated point)

The non-irradiated points shows an higher gain compared to the irradiated one because they suffered only from the effect of the kapton polarization that results only in a gain

increase. In the long time irradiated point the two effects sum up resulting in a lower gain: the increase given by the kapton polarization is contrasted by radiation effects.

The fact that the radiation effects results in a gain decrease is confirmed by *on before measurements*. Figure 6.5 shows the result for two different rates

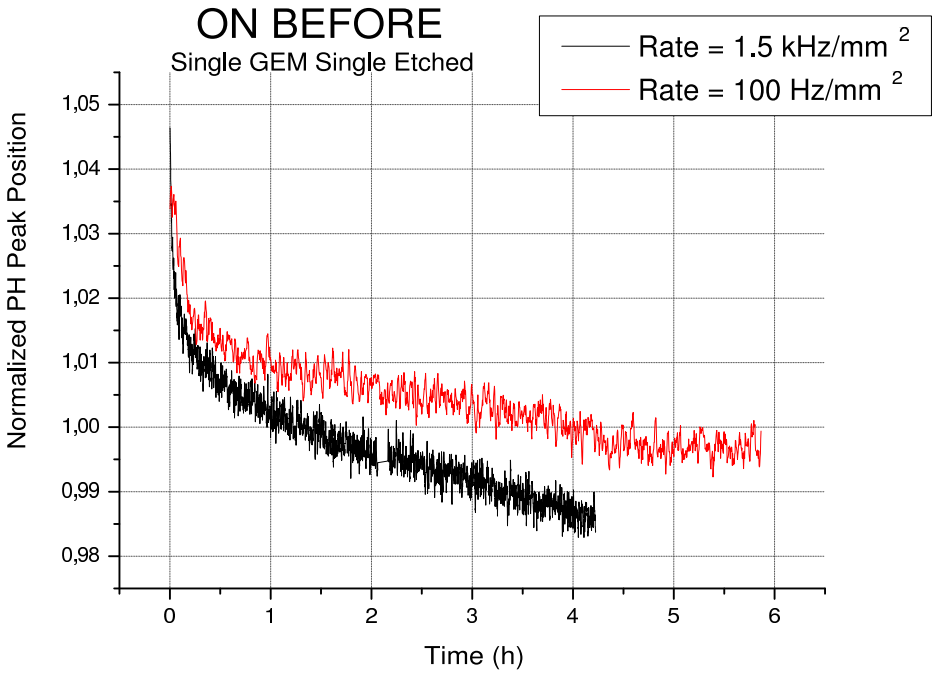

Figure 6.5: The radiation effects results in a gain decrease. In particular the higher the rate the faster is the decrease

The gain decrease due to the radiation effect is again confirmed. In particular higher rates result in a faster gain decrease. A plateau is reached after 6 hours. All the variations are less than 10%.

All the previous measurements were performed irradiating the chamber from the front. A final analysis was performed to understand if irradiating the chamber from different angles imply different consequences. It is important to explain what is the difference in irradiating the chamber from the front (angle of 0 degrees, radiation direction perpendicular to kapton window) or from the side (angle of 90 degrees, radiation direction parallel to kapton window). If the chamber is irradiated from the front the X-rays enter the detector through the mylar window and have a very high probability to hit and convert in the copper or in the kapton. On the contrary if the detector receives the radiation from the side, the X-Rays enter the detector

through a little lateral slit and will convert in the drift region, with a very small probability to hit the electrodes. All the analysis was performed doing *same time measurements*. Figure 6.6 illustrates the result.

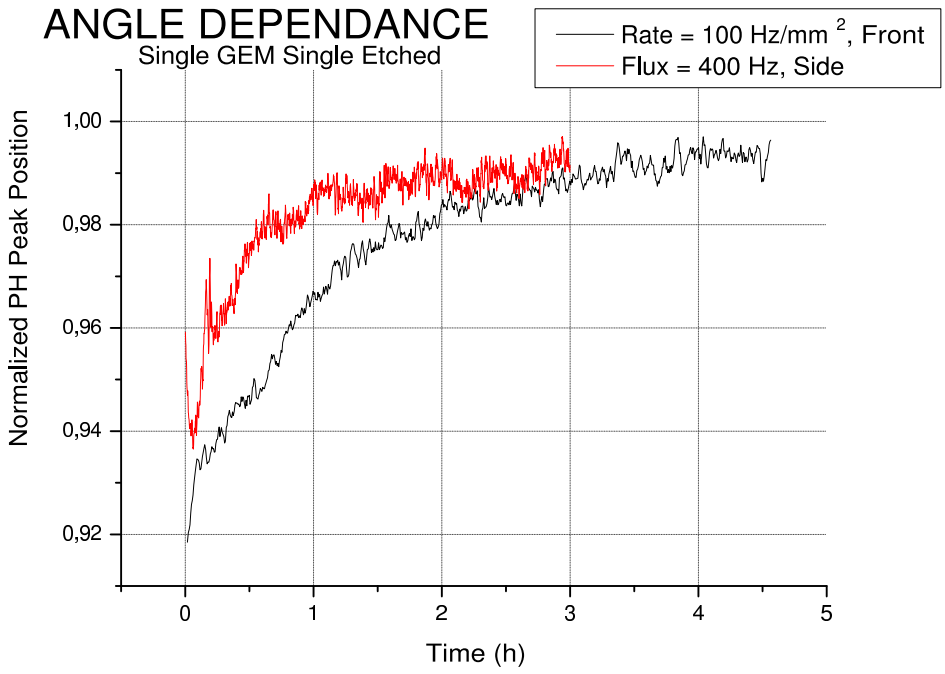

Figure 6.6: The angle dependence seems to imply only a different initial behaviour.The flux is defined as the integral of the rate over the detector surface; it is not possible to define a rate for the side-shooting measurement because the detector irradiation area can not be determined

In principle different shooting angle permits to study the influence of the photons conversion in solid material. Shooting from the side implies an initial gain decrease, a behaviour very similar to the high rate *same time measurement*. Since the conversion probability has an exponential shape, it is higher in the part of the drift region nearest to the source ant thus it is probable that in this region the rate was very high resulting in a gain decrease at the beginning. Then after a while the kapton polarization overtook yielding a gain increase. All the variations are always less than 10%.

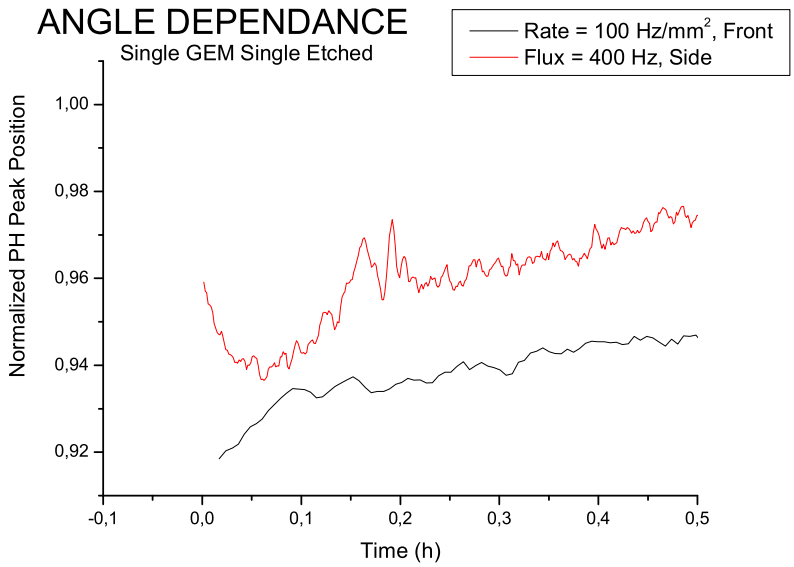

Figure 6.7: Zoom of the firsts 30 minutes of Fig. 6.6

6.7.1 Different kinds of GEMs

The previous analysis suggests that the standard geometry has a small instability. Precedent studies suggested that the gain modification can be due to the shape of the holes. In order to verify this assumption other two kinds of GEMs with different holes shapes and geometry were tested: the double etched and the triple etched GEM. Double and triple etched can be obtained starting from the standard geometry (single etched) and leaving the foil in the kapton etching liquid for twice (double) or three times (triple etched) the time. These two geometries have different kapton holes and the values the hole parameters are reported in Table 6.7.1.

Type of Etching	**Kapton Diameter**	**Copper Diameter**
Single	50 μm	70 μm
Double	60 μm	70 μm
Triple	70 μm	70 μm

An exaggerated view of the shapes of the holes is shown in Fig 6.8

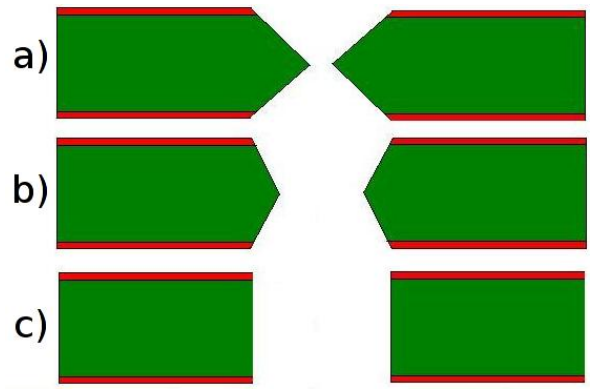

Figure 6.8: Approximate Cross section view of the three geometries: a) single etched (standard), b) double etched, c) triple etched (cylindrical)

6.7.2 Different geometries

The three different geometry were compared performing a *same time measurement* The results are shown in Fig 6.9

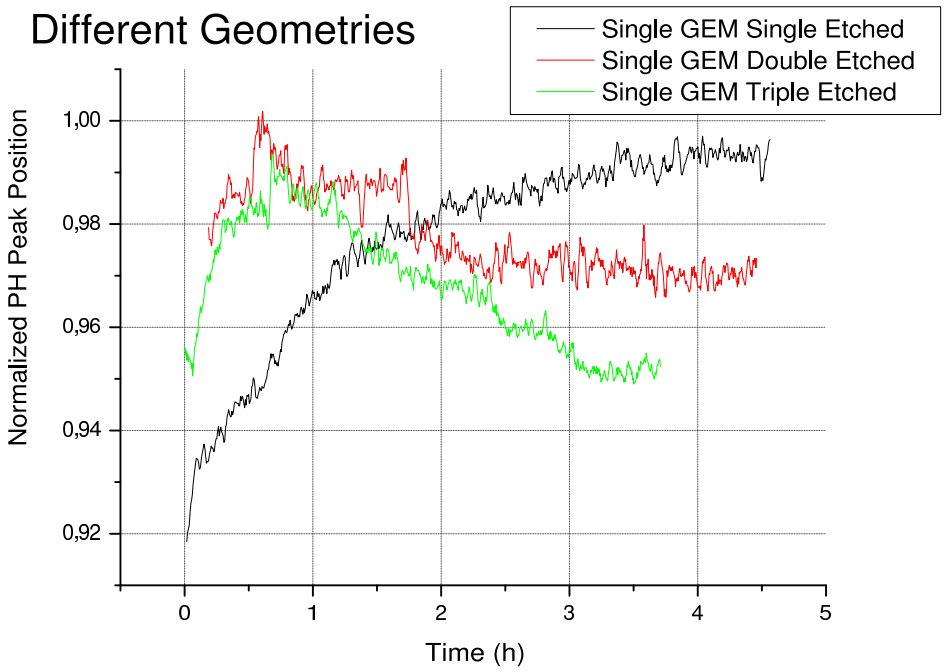

Figure 6.9: Comparison between the three geometries. The rate was always 100 Hz/mm^2. All *Same Time Measurements*

For the new GEM types the gain variation are in the 10% range. The standard geometry shows an initial gain increase and reaches the plateau after approximately 5 hours. The double etched geometry seems to be the more stable while the cylindrical one shows an initial increase followed by a decrease. The time constants of the three effects are different for the three geometries.

The naive argument that the most stable geometry should be the one with the ratio between copper hole diameter and kapton diameter as close as possible to one seems not to be confirmed.

6.8 Triple GEM Analysis

The experimental setup used was always the one described in Chapter 4 and a resistor divider (see Fig 4.5) was used to supply the voltage to the chamber. All the gaps were 2 mm large except the drift gap that was 3 mm. Putting -3800V on the Vcc input, each GEM has a potential difference around 320 V. The three effects shown in general the same results as for the single GEM structure: the kapton polarization imply a gain increase while the radiation effect a decrease but the values of gain variations were higher than the single structure. Here only studies that differ from the ones performed on the single GEM structure are reported.

6.8.1 Gain Rate Stability

The gain stability in function of the rate was studied. Figure 6.10 shows the results of this analysis.

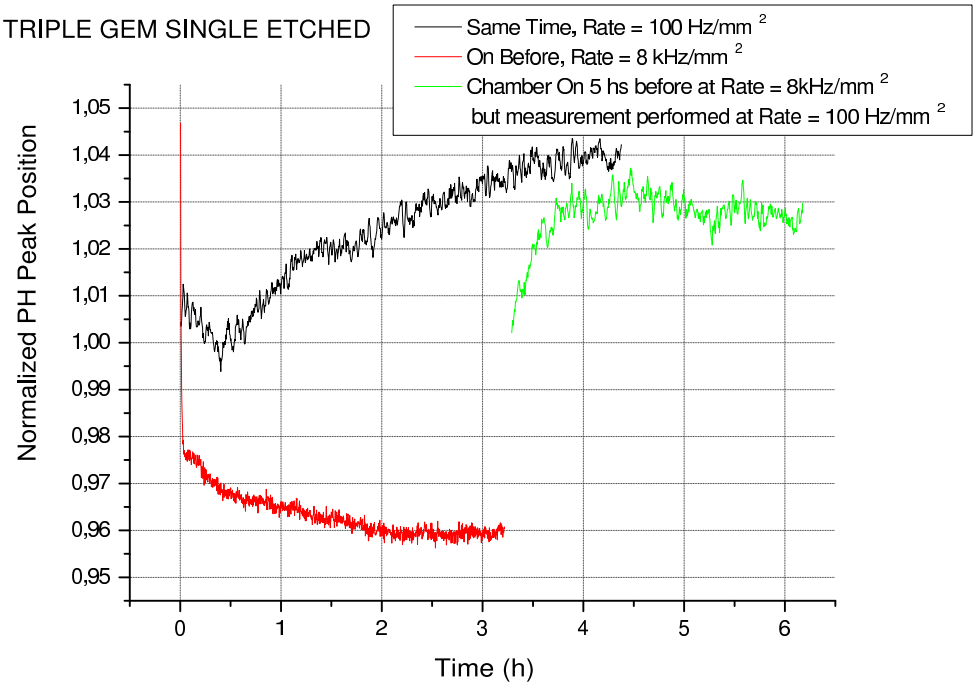

Figure 6.10: The gain rate stability study

The red curve is a high rate *on before measurement* and the black one is a low rate *same time measurement* The green curve is the result obtained leaving the chamber with high voltage applied and strongly irradiated (8 kHz/mm^2) for few hours and then changing the rate to 100 Hz/mm^2: the gain comes back to the 100Hz/mm^2 equilibrium line. It means that each irradiation rate may have a specific equilibrium line. If this is true the GEM may not have a perfect uniform response in a TPC endcap but it is important to underline that this gain rate variation is always small, around 10%

6.8.2 Different geometries

Apart the standard geometry only the double etched one was tested in the triple GEM structure. Figure 6.11 shows the comparison between the two *On Before Measurements*. The double etched has a faster gain loss and stabilize on an equilibrium line that is lower than the one for single etched.

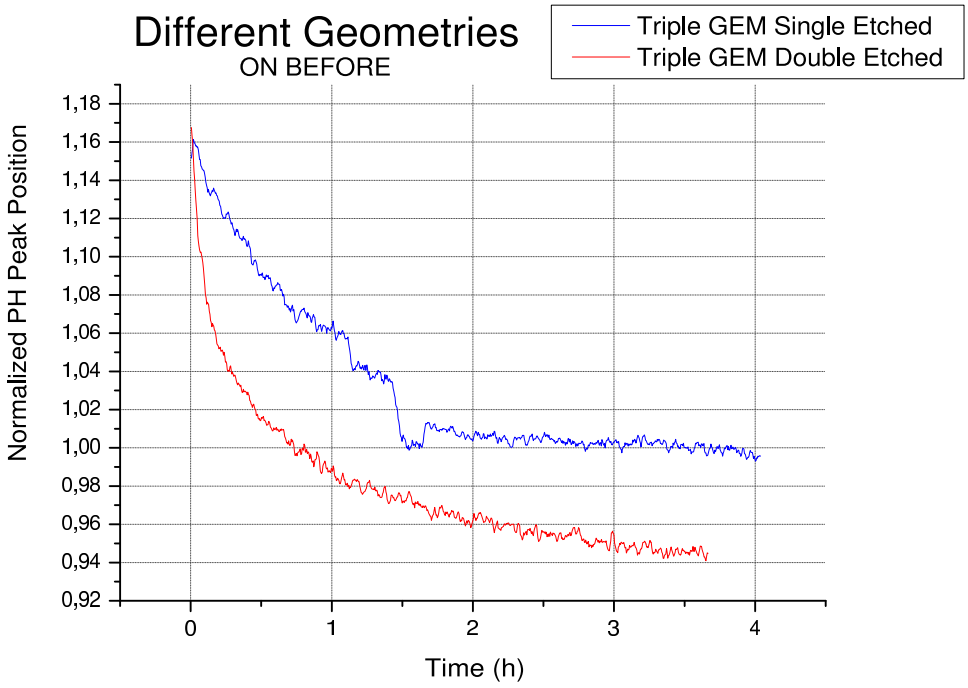

Figure 6.11: Comparison between Triple Gem Single Etched and Double Etched

6.9 Triple and Single GEM comparison

The aim of this study is to understand if the behaviour of the triple GEM can be deduced by the behaviour of the individual GEMs composing the structure. The three GEMs were tested alone performing an *on before measurement* and then their normalized pulse height peak positions were multiplied to see if the single GEM multiplication has the same behaviour of the triple GEM. Figure 6.12 shows the result of this exercise.

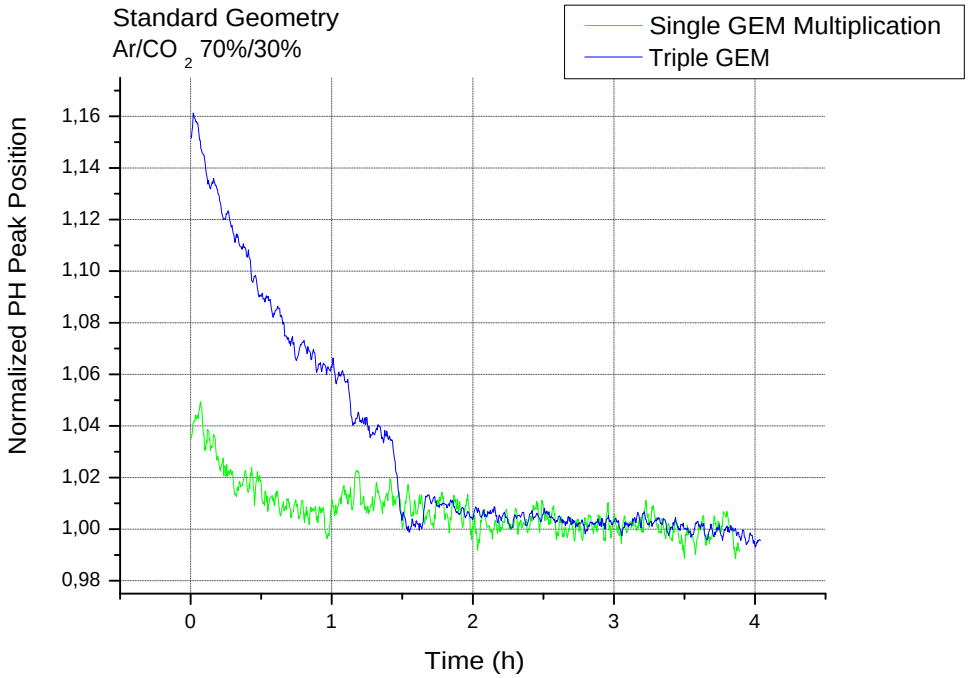

Figure 6.12: The comparison between the triple GEM structure and the multiplication of the three singles GEM

It is evident that the behaviour is different: the explanation can be that the effect on gain of similar charge deposits depends non on the total gain but on the voltage of each foil.

Chapter 7

GEM applications in medical field

Owing to their excellent position resolution and rate capability GEM-based detector are very suitable to be used in different applications: from the high energy physics to the medical imaging field. One of the first study for applications in this field was the radiography of a small mammal with a Multi-GEM detector equipped with a 2D readout. Figure 7.1 shows the results.

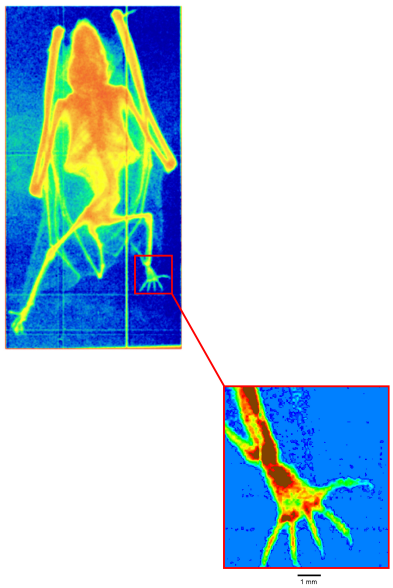

Figure 7.1: X-Ray Absorption Image of a small mammal, [BKK+02]

The second major subject of this report is the study of a new kind of GEM-based detector

for application in medical physics.

7.1 Depth of Interaction Determination in GEM-based multilayer PET detectors

This detector is a new concept of GEM-based detector that will be used in PET applications.

The objective of this new device is the detection and localization of high energy photons making use of an appropriate converter sheet in front of a GEM device used for charge amplification. To compensate for the low conversion efficiency of a single element, multilayer structures are needed, with stacks of converter-GEM modules; alternatively the same GEM electrode can be used as converter. Each elementary cell of this detector is composed by a converter followed by a GEM foil. Figure 7.2 represents a schematic view of two cells of this detector.

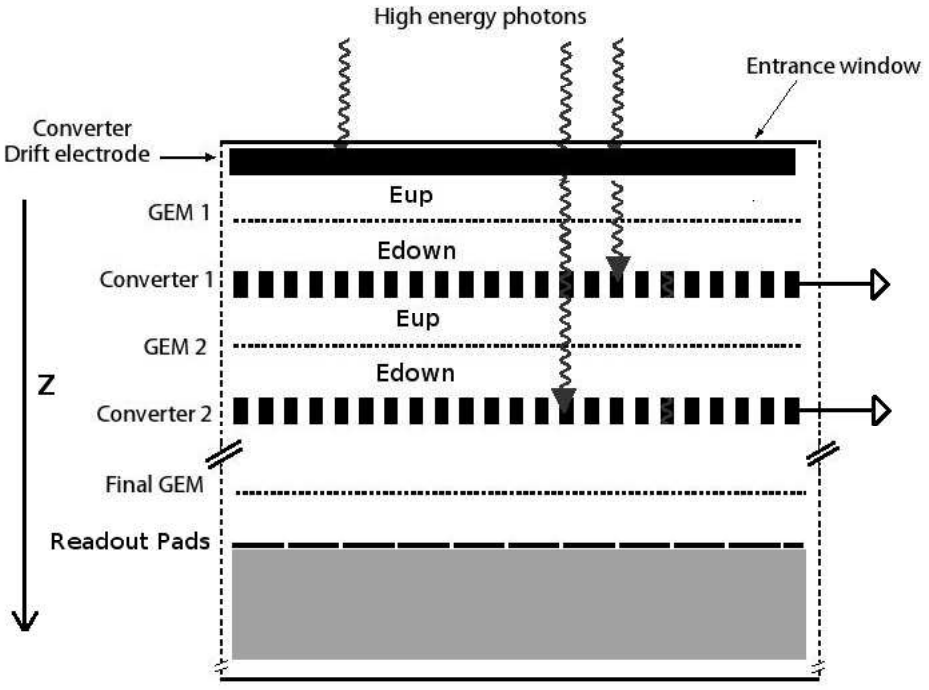

Figure 7.2: Schematic view of some cells of this new kind of detector (taken but modified from [Ö06])

The high energy photons enter through the entrance window and can convert in one of the converters. The drift electrode will be itself a converter. Ionization charge released by the photoelectron coming from photon conversion is transported through the structure into a position-sensitive terminal GEM detector and to a readout pads board. In this way it is mandatory that converters were meshes in order to let a part of the charge pass through. Detailed simulation studies have been done to compute efficiencies and optimize the geometry of such structures

Two fundamental limitations can hinder the use of this technology:

1. In a multi-layer GEM-converted stack, one has to ensure that the charge transported to the final multiplier does not depend on the conversion depth

2. The thickness of each cell, typically several mm, adds an (unknown) delay to the final charge collection, implying a poor time resolution; for ten cells, this would be of several hundred ns, seriously restricting the use of the device.

The first requirement is easy to satisfy, simply choosing the values of field and GEM voltages for which the effective gain of each cell is unitary. To solve the second problem, we have designed a structure where, while the effective gain in each cell is large and allows direct detection of a signal to determine the interaction layer, the amount of charge transferred to the next cell is strongly reduced, so that the overall charge transfer is unitary.

The three coordinates of photon conversion point are then measured separately. The depth, the z coordinate (see Fig 7.2) is measured knowing which layer is the first to give a signal: it means that the photon converted on the immediately previous converter. The other two coordinates are recorded by strips or pads on the last electrode of the structure.

This report describes preliminary results obtained with a structure that permits to overcome the limitations.

7.2 The two cells test detector

7.2.1 Experimental Setup

The detector that was used for the measurements was composed by two cells of the final detector. Figure 7.3 illustrates this test detector. The second converter was substituted by a full plate used as final readout anode. The two elementary cells are represented by the Top

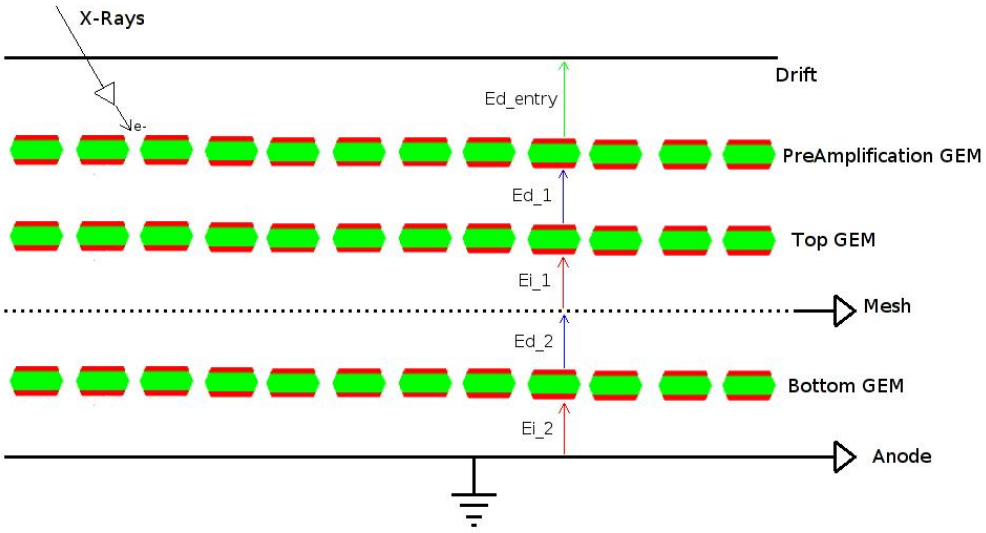

Figure 7.3: Experimental Setup

GEM plus the mesh and the Bottom GEM plus the anode. An additional multiplier GEM foil with a drift gap above the GEM-converter pair was used to have the possibility to inject a controlled and higher amount of charge into this test detector.

The GEM foils used were standard GEM foils (70 μm hole diameter and 140 μm pitch and an active area of 10x10 cm^2); the converter was a 10 μm thick copper foil, chemically pierced with 50μm diameter holes at 400 μm pitch. The optical transparency of this mesh was around 1.2%. Figures 7.4 and 7.5 show pictures of GEMs and mesh used.

The radioactive sources used were an uncollimated ^{55}Fe and the X-Ray generator producing copper X-rays. The gas mixture used throughout the measurements was Ar/Co_2 70%/30%. The different electrodes were powered using separate HV power supply.

7.2.2 Basic Principle

The requirement of cell unitary gain is experimentally satisfied finding out conditions of electric fields and potential differences on the GEMs (with GEMs I mean through all this report the Top and Bottom GEMs) that give the same signal on the mesh and on the anode. Since every cell must be identical to the others, the condition to have the two cell of the detector identical is to have the same potential difference on the GEM and same electric fields. Using the nomenclature of figure 7.3 a mathematical way to express all these requests is:

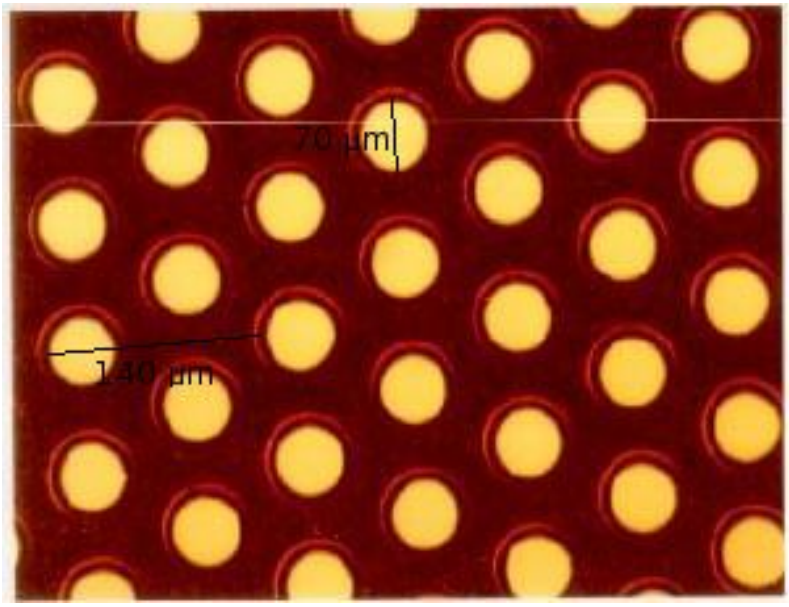

Figure 7.4: Photos of the GEM foil used

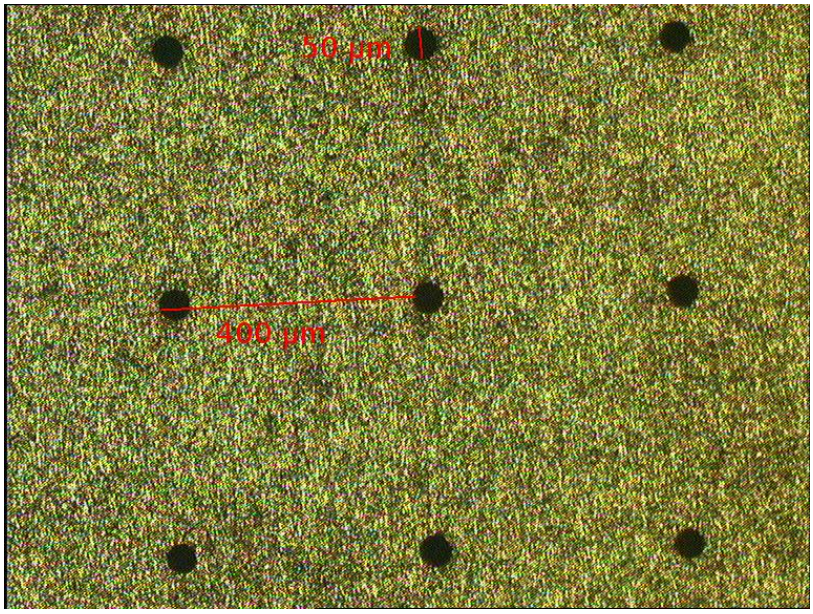

Figure 7.5: Photo of mesh foil used

$$E_{d1} = E_{d2} = E_d \tag{7.1}$$

$$E_{i1} = E_{i2} = E_i \tag{7.2}$$

$$\Delta V_{TopGEM} = \Delta V_{BottomGEM} = \Delta V_{GEM} \tag{7.3}$$

The conditions expressed in 7.1, 7.2 and 7.3 imply that

$$G_{Eff,TopGEM} = G_{Eff,BottomGEM} = G_{Eff} \tag{7.4}$$

and thus the unitary cell total effective gain is achieved if

$$\epsilon_{mesh} = \frac{1}{G_{Eff}} \tag{7.5}$$

where ϵ_{mesh} is defined as the mesh electron transparency.

7.2.3 Measurements

Since it was necessary to acquire two independent signals from the mesh and from the anode (see Fig 7.3), these two electrodes were provided with two calibrated electron chains with equal electron gain

The parameters that play a fundamental role to define a unitary cell gain are the ratio between the induction and drift fields and the potential difference of the Top and Bottom Gem. The value of the preamplifier GEM potential difference and of the entrance drift field were adjusted to have good signals. Respecting all the requirements the measurement performed consisted in fixing the sum and the ratio of the two fields and vary the GEMs potential difference.

Only two different fields sums and ratios were tested: $E_i + E_d = 3.7$ KV/cm, $E_i/E_d = 5$ and $E_i + E_d = 2.1$ KV/cm, $E_i/E_d = 20$

The reason why the GEM voltage plays a very important role is explained by simple calculations. If G_{Eff} the effective gain of the GEMs and ϵ_{mesh} the mesh electron transparency the ratio between the anode (S_{anode}) and the mesh (S_{mesh}) signals is

$$\frac{S_{anode}}{S_{mesh}} = \epsilon_{mesh} \cdot G_{Eff} \tag{7.6}$$

Since the effective gain depends very strongly on GEM potential difference the signal ratio will have the same strong dependence. The results of the measurement are shown in Figure 7.6. The strong signal ratio dependence on the GEM potentials is confirmed.

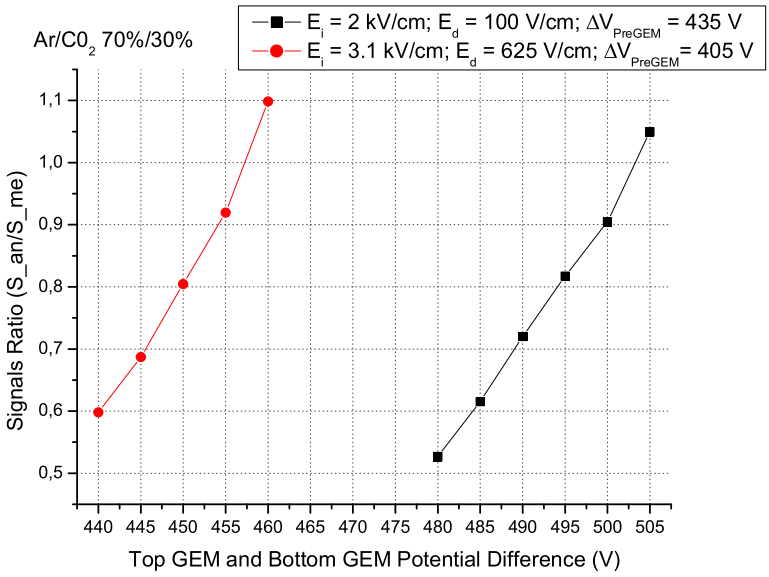

Figure 7.6: Signal Ratio Vs potential difference on the GEMs

Reducing the field sum and increasing the ratio drive to allow to achieve the unitary signal ratio at an higher GEM voltage difference.

The current best parameters that satisfy the requirements are

$$\Delta V_{GEM} = 500V$$

$$E_d = 100V/cm$$

$$E_i = 2KV/cm$$

For the other fields configuration the unitary signals ratio was found around 455 V.

Plots 7.7 shows the pulse height spectra acquired on the mesh and on the anode at the best situation. It is important to remark that the anode and mesh energy resolution remain anyway around 30%.

7.2.4 Results Evaluation

To verify if the model describes well the measurements it is necessary to verify equation 7.5 measuring separately the effective gain and the mesh electron transparency at the unitary gain conditions found.

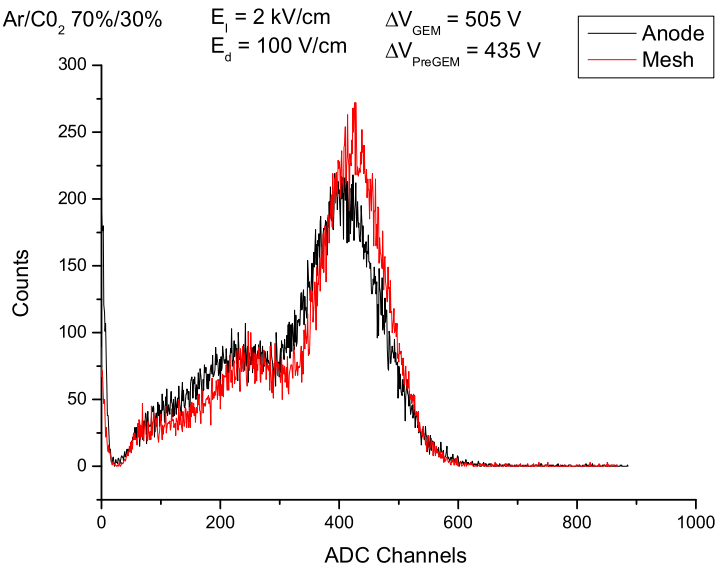

Figure 7.7: Pulse height spectra acquired on the two electrodes at the best conditions. The signal peak positions ratio is very near to one

Effective GEMS Gain Measurement

The effective gain of the two GEMs was measured using formula 5.1. Both the Top and Bottom GEM gain was measured and very similar results were found. Figure 7.8 shows the gain measurement for the two fields conditions.

Knowing what is the gain corresponding to a particular fields configuration and potentail difference on the GEMs it is possible to express the signal ratio in function of the effective GEM gain. Figure 7.9 shows the result of this exercise

The lowest field sum condition seems to have GEM gain around 380 and the highest one around 240.

Mesh Electronic Transparency Measurement

The experimental setup used to measure the mesh electron transparency is shown in Fig 7.10. No amplification devices were used and the currents were simple ionization currents.

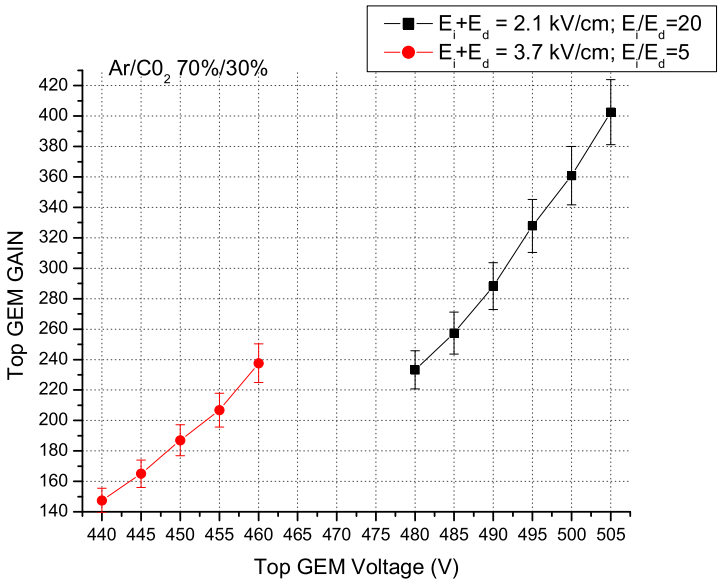

Figure 7.8: Top GEM Gain measurement

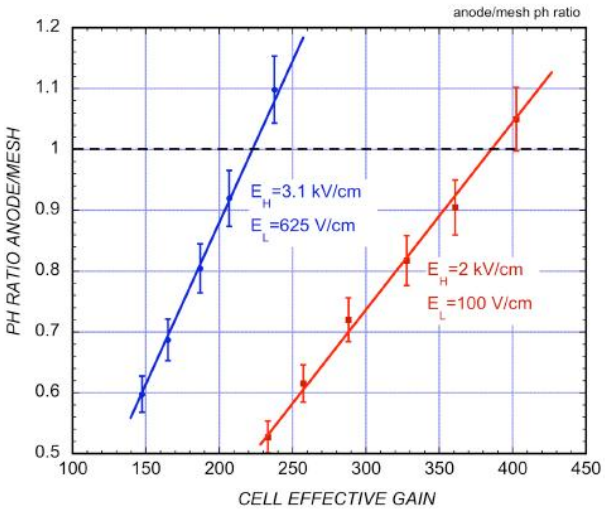

Figure 7.9: Signals Ratio VS the Top GEM effective gain, E_H is the Induction Field and E_L the Drift Field

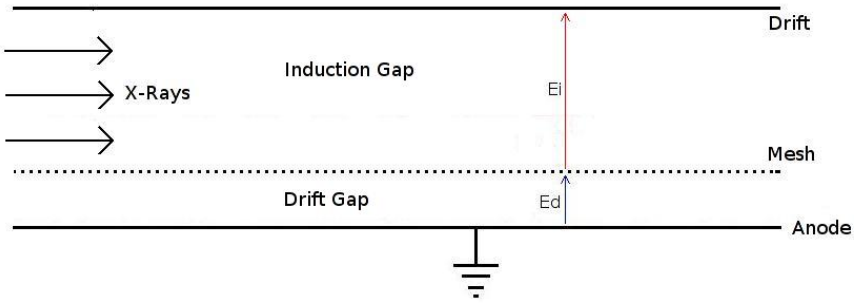

Figure 7.10: Experimental Setup to measure the mesh electron transparency. It is important to have a large conversion gap to avoid the possibility to have conversions in the region below the mesh

The X-Rays enter from a slit on the side of the detector and convert in the region between the drift and the mesh. In agreement with the previous nomenclature this region is called induction region. The electron transparency depends on the ratio between the induction field (E_i, the one before the mesh) and the drift field (E_d, the one after the mesh) and is calculated as:

$$\epsilon_{mesh} = \frac{I_{Anode}}{I_{Drift}} \tag{7.7}$$

Plot 7.11 shows the results of the measurements of the electron transparency in a gas mixture of Ar/Co_2 70%/30% in the previously described fields conditions

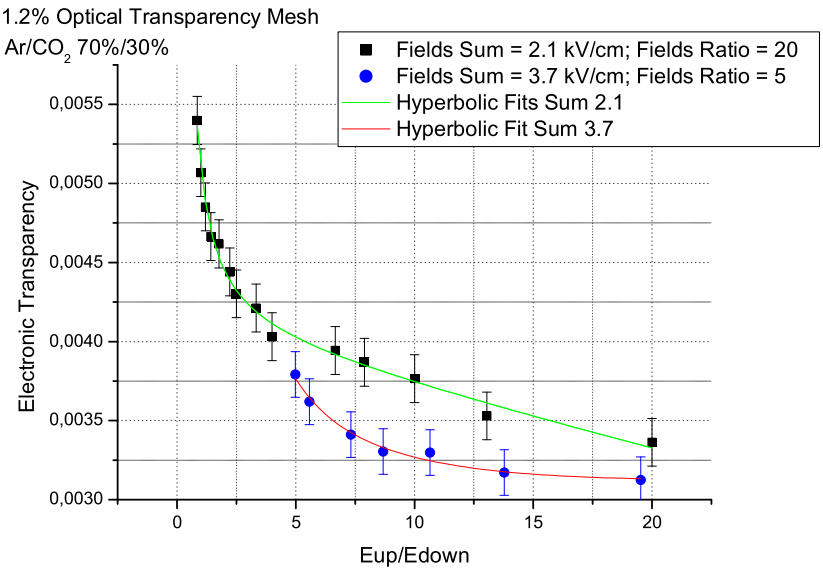

Figure 7.11: Mesh electron transparency measurement. E_{up} represents the induction field

The mesh electron transparency measured at first field conditions that yields the unitary cell gain ($E_i/E_d = 20$,E_i+E_d = 2.1 kV/cm) is around 0.0032 yielding a GEM effective gain of around 300. For the other unitary cell condition ($E_i/E_d = 5$) the electron transparency is around 0.0038 giving a GEM gain around 260.

7.3 Summary

The two measurements yield the following values for the GAIN and mesh electron transparency:

1) $E_i + E_d = 2.1$ KV/cm, $E_i/E_d = 20$, $\Delta V_{GEM} \simeq 500$ V:

GAIN $= 380 \pm 20$; $1/\epsilon = 300 \pm 20$

2) $E_i + E_d = 3.7$ KV/cm, $E_i/E_d = 5$, $\Delta V_{GEM} \simeq 455$ V:

GAIN $\simeq 240 \pm 10$; $1/\epsilon \simeq 260 \pm 14$

The conclusion is that the two measurements (GAIN and Electron Transparency) for both fields configuration were compatible and that formula 7.5 was verified.

Bibliography

[ABBM+04] A Andronic, S F Biagi, P Braun-Munzinger, C Garabatos, and G Tsiledakis. Drift velocity and gain in argon- and xenon-based mixtures. *Nucl. Instrum. Methods Phys. Res., A*, 523(physics/0402044):302–308. 11 p, Feb 2004.

[ADK+01] M C Altunbas, K Dehmelt, S Kappler, B Ketzer, Leszek Ropelewski, Fabio Sauli, and F Simon. Aging measurements with the gas electron multiplier (gem). *Nucl. Instrum. Methods Phys. Res., A*, 515(CERN-EP-2001-091. 1-2):249–254. 6 p, Dec 2001.

[AFPS03] G Auriemma, D Fidanza, G Pirozzi, and C Satriano. Experimental determination of the townsend coefficient for argon-co2 gas mixtures at high fields. *Nucl. Instrum. Methods Phys. Res., A*, 513(physics/0307073):484–489, Jul 2003.

[BBB+97] J M Benlloch, A Bressan, C Bttner, M Capans-Garrido, M Gruw, M Hoch, J C Labb, Alfredo Placci, Leszek Ropelewski, Fabio Sauli, A Sharma, and R Veenhof. Development of the gas electron multiplier (gem). (CERN-PPE-97-146):11 p, Nov 1997.

[BBCG+98] J M Benlloch, A Bressan, M Capans-Garrido, M Gruw, M Hoch, J C Labb, Alfredo Placci, Leszek Ropelewski, and Fabio Sauli. Further developments of the gas electron multiplier (gem). (CERN-EP-98-050):11 p, Mar 1998.

[BBCG+00] S Bachmann, A Bressan, M Capans-Garrido, M Deutel, S Kappler, B Ketzer, A Polouektov, Leszek Ropelewski, Fabio Sauli, E C Schulte, L I Shekhtman, and A Sokolov. Discharge studies and prevention in the gas electron multiplier (gem). *Nucl. Instrum. Methods Phys. Res., A*, 479(CERN-EP-2000-151. 2-3):294–308. 25 p, Dec 2000.

[BBK+00] S Bachmann, A Bressan, B Ketzer, M Deutel, Leszek Ropelewski, Fabio Sauli, A E Bondar, A F Buzulutskov, L I Shekhtman, A Sokolov, A A Tatarinov, A Vasilev, S Kappler, and E C Schulte. Performance of gem detectors in high intensity particle beams. *Nucl. Instrum. Methods Phys. Res., A*, 470(CERN-EP-2000-116. 3):548–561. 33 p, Aug 2000.

[BBK+01] S Bachmann, A Bressan, B Ketzer, M Deutel, Leszek Ropelewski, Fabio Sauli, S Kappler, and E C Schulte. Optimisation of the gas electron multiplier for high rate applications. *Nucl. Instrum. Methods Phys. Res., A*, 461(1-3):42–46, 2001.

[BBR+99] S Bachmann, A Bressan, Leszek Ropelewski, Fabio Sauli, A Sharma, and D Mrmann. Charge amplification and transfer processes in the gas electron multiplier. oai:cds.cern.ch:cern-ep-99-048. *Nucl. Instrum. Methods Phys. Res., A*, 438(CERN-EP-99-048):376–408. 45 p, Apr 1999.

[Bia99] S F Biagi. Monte carlo simulation of electron drift and diffusion in counting gases under the influence of electric and magnetic fields. *Nucl. Instrum. Methods Phys. Res., A*, 421(1-2):234–240, 1999.

[BKK+02] S Bachmann, S Kappler, B Ketzer, T Mller, Leszek Ropelewski, Fabio Sauli, and E C Schulte. High rate x-ray imaging using multi-gem detectors with a novel readout design. *Nucl. Instrum. Methods Phys. Res., A*, 478(1-2):104–8, 2002. Ninth International Vienna Conference on Instrumentation 2001, Vienna, Austria, 19-23 Feb. 2001. , In: Nuclear-Instruments-Methods-in-Physics-Research-Section-A (Accelerators, Spectrometers, Detectors and Associated Equipment) (Netherlands), vol.4.

[BMRS99] A Bressan, D Mrmann, Leszek Ropelewski, and Fabio Sauli. Gem detector at work. *Nucl. Phys. B, Proc. Suppl.*, 78:389–94, 1999.

[BRSM00] A Bressan, Leszek Ropelewski, Fabio Sauli, and D Mrmann. Development of high gain gem detectors. *IEEE Trans. Nucl. Sci.*, 47(6, pt.2):2070–4, 2000.

[BSB+99] A F Buzulutskov, L Shekhtman, A Bressan, A D Mauro, Leszek Ropelewski, Fabio Sauli, and S F Biagi. Gem operation in pure noble gases and the avalanche confinement. *Nucl. Instrum. Methods Phys. Res., A*, 433(1-2):471–475, 1999.

[Eve06] Pieter Everartes. Rate capability and ion feedback in gem-detectors. Master's thesis, Universiteit Gent, Facultait Ingenierswetenschappen, 2005-2006.

[KAD+01] B Ketzer, M C Altunbas, K Dehmelt, J Ehlers, J M Friedrich, B Grube, S Kappler, I Konorov, S Paul, Alfredo Placci, Leszek Ropelewski, and Fabio Sauli. Triple gem tracking detectors for compass. *IEEE Trans. Nucl. Sci.*, 49(CERN-OPEN-2002-004. 5 pt.2):2403–10. 16 p, Dec 2001.

[Kap04] Stefen Kappler. *Development of a GEM-based TPC readout for future collider experiment.* PhD thesis, IEKP, Karlsruhe University, 2004.

[Kno99] *Radiation Detection and Measurement, 3rd Edition.* John Wiley and Sons, Inc, 1999.

[MRS04] T Meinschad, Leszek Ropelewski, and Fabio Sauli. Gem-based photon detector for rich applications. oai:cds.cern.ch:cern-ph-ep-2004-015. *Nucl. Instrum. Methods Phys. Res., A*, 535(CERN-PH-EP-2004-015. 1-2):324–329. 9 p, Apr 2004.

[Ö06] Janina Östling. *New efficient detector for radiation therapy imaging using Gas Electron Multipliers.* PhD thesis, 2006.

[Rop06] Leszek Ropelewski. Gem at cern, detector seminar. Technical report, http://leszek.home.cern.ch/leszek, 2006.

[Sau77] Fabio Sauli. Principles of operation of multiwire proportional and drift chambers. page 92 p, Geneva, May 1977. CERN, CERN. CERN, Geneva, 1975 - 1976.

[SFG+02] F Simon, J M Friedrich, B Grube, I Konorov, S Paul, M C Altunbas, S Kappler, B Ketzer, A Placci, Leszek Ropelewski, and Fabio Sauli. Gem detectors for compass. 2002.

[Sta00] M. A. Stanley. *Sprites and their parent discharges.* PhD thesis, New Mexico institute of Mining and Technology, 2000.

[TV02] V Tikhonov and R Veenhof. Gem simulation methods development. *Nucl. Instrum. Methods Phys. Res., A*, 478(1-2):452–9, 2002. Ninth International Vienna Conference on Instrumentation 2001, Vienna, Austria, 19-23 Feb. 2001. ,

In: Nuclear-Instruments-Methods-in-Physics-Research-Section-A (Accelerators, Spectrometers, Detectors and Associated Equipment) (Netherlands), vol.4.

[Vee06] R Veenhof. Photon detection in a gas. *Nucl. Instrum. Methods Phys. Res., A*, 563:291–298, 2006.

[Vee07] Rob Veenhof. Diffusion in strongly convergent and divergent fields. Technical report, http://consult.cern.ch/writeup/garfield/notes/diffusion.ps, 2007.